J. Fluid Mech. (1994), *vol.* 280, *pp.* 119–148

Gravity-induced coalescence of drops at arbitrary Péclet numbers

By ALEXANDER Z. ZINCHENKO AND ROBERT H. DAVIS†
Department of Chemical Engineering, University of Colorado, Boulder, CO 80309-0424, USA

(Received 20 December 1993 and in revised form 15 June 1994)

The collision efficiency in a dilute suspension of sedimenting drops is considered, with allowance for particle Brownian motion and van der Waals attractive force. The drops are assumed to be of the same density, but they differ in size. Drop deformation and fluid inertia are neglected. Owing to small particle volume fraction, the analysis is restricted to binary interactions and includes the solution of the full quasi-steady Fokker–Planck equation for the pair-distribution function. Unlike previous studies on drop or solid particle collisions, a numerical solution is presented for arbitrary Péclet numbers, Pe, thus covering the whole range of particle size in typical hydrosols. Our technique is mainly based on an analytical continuation into the plane of complex Péclet number and a special conformal mapping, to represent the solution as a convergent power series for all real Péclet numbers. This efficient algorithm is shown to apply to a variety of convection–diffusion problems. The pair-distribution function is expanded into Legendre polynomials, and a finite-difference scheme with respect to particle separation is used. Two-drop mobility functions for hydrodynamic interactions are provided from exact bispherical coordinate solutions and near-field asymptotics. The collision efficiency is calculated for wide ranges of the size ratio, the drop-to-medium viscosity ratio, and the Péclet number, both with and without interdroplet forces. Solid spheres are considered as a limiting case; attractive van der Waals forces are required for non-zero collision rates in this case. For $Pe \gg 1$, the correction to the asymptotic limit $Pe \to \infty$ is $O(Pe^{-1/2})$. For $Pe \ll 1$, the first two terms in an asymptotic expansion for the collision efficiency are $C/Pe + \frac{1}{2}C^2$, where the constant C is determined from the Brownian solution in the limit $Pe \to 0$. The numerical results are in excellent agreement with these limits. For intermediate Pe, the numerical results show that Brownian motion is important for $Pe \leqslant O(10^2)$. For $Pe = 10$, the trajectory analysis for $Pe \to \infty$ may underestimate the collision rate by a factor of two. A simpler, approximate solution based on neglecting the transversal diffusion is also considered and compared to the exact solution. The agreement is within 2–3 % for all conditions investigated. The effect of van der Waals attractions on the collision efficiency is studied for a wide range of droplet sizes. Except for very high drop-to-medium viscosity ratios, the effect is relatively small, especially when electromagnetic retardation is accounted for.

1. Introduction

Numerous theoretical investigations have been made in recent years to calculate the collision efficiency in a dilute suspension of sedimenting spheres. For typical hydrosols with particles generally smaller than 50 μm, the fluid and particle inertia can usually be

† To whom correspondence should be addressed.

neglected, as can drop deformation. On the other hand, a comprehensive physical model for the collision process should necessarily include van der Waals attractive forces and Brownian motion. Van der Waals attractions, being singular when two particles touch, play a crucial role in the collision of highly viscous drops and are required for the aggregation of solid smooth spheres, owing to the high hydrodynamic resistance of the lubrication liquid layer between two nearly touching surfaces (Davis 1984). The gravity-induced relative motion with respect to Brownian relative motion is measured by the Péclet number, Pe, which is proportional to the fourth power of particle size (Zhang & Davis 1991). Typical hydrosol particles ranging from 0.5 to 5 μm in size may therefore have a broad range of Péclet numbers, from small to high values. However, to the best of our knowledge, only the limiting cases $Pe \ll 1$ and $Pe \gg 1$ have been rigorously considered so far.

Spielman (1970) developed a theoretical model to predict the rate of coagulation for monodispersed rigid spheres subject to Brownian diffusion only ($Pe = 0$). Valioulis & List (1984) and Kim & Zukovski (1990) performed similar calculations for heterodispersed rigid spheres. Melik & Fogler (1984*a*) derived a two-term asymptotic expansion for the collision efficiency of rigid spheres at $Pe \ll 1$ by matched asymptotic expansions. Wang & Wen (1990) extended their calculations and obtained a four-term asymptotic expansion, in a manner very similar to that used by Acrivos & Taylor (1962) for heat or mass transfer to a sphere at small Péclet number. For gravity-induced coagulation of rigid spheres without Brownian diffusion ($Pe = \infty$), theoretical models have been developed by Davis (1984) and Melik & Fogler (1984*b*) to predict the rate of coagulation using trajectory analyses, and by Wen & Batchelor (1985) using an asymptotic approach to the convection–diffusion equation at $Pe \to \infty$. As expected for correct two-sphere hydrodynamics, all of these studies show that the hydrodynamic resistance to relative motion causes the collision rates to approach zero as the attractive forces become weak.

For spherical non-Brownian drops, Zinchenko (1982) calculated the collision efficiency by a trajectory analysis, without considering the effects of interparticle attraction. The finite collision efficiency in this case is due to a weaker singularity of the hydrodynamic resistance when the drops approach each other, in comparison to the case of solid spheres. Zhang & Davis (1991) included the effects of van der Waals forces and also considered the other limiting case of strong Brownian diffusion, $Pe = 0$. In all of these studies, the results of well-advanced theories for two-drop hydrodynamic interactions were used, including exact bispherical coordinate solutions for the motion along (Rushton & Davies 1973; Haber, Hetsroni & Solan 1973) and normal (Zinchenko 1980) to the line-of-centres and near-field asymptotic solutions for small separations (Zinchenko 1978, 1982; Davis, Schonberg & Rallison 1989).

The main objective of the present work is to calculate exactly the gravity-induced collision efficiency for two unequal drops with and without van der Waals attraction at arbitrary Péclet number, thus covering the whole range of particle size in typical hydrosols. The limiting case of solid spheres at arbitrary Pe is included. In §2, the problem is formulated as the solution of the full quasi-steady, Fokker–Planck (FP) equation for the pair distribution function, $p(\boldsymbol{r})$. In lieu of matched asymptotic expansions (Wang & Wen 1990), which can provide a remarkable accuracy for small $Pe \neq 0$, but, unfortunately, fail quickly as the Péclet number grows (see §6), we offer an efficient numerical technique valid for aribitrary Pe (§3). After the boundary condition at infinity has been transferred to some remote, but finite sphere, the problem becomes one of regular perturbations and, in principle, the solution can be expanded in powers of Pe. Obviously, the radius h of convergence is small (and tends to zero,

when the position of the outer boundary tends to infinity), and so in practice this expansion cannot be used for finite Pe. However, all the singularities for this expansion in the plane of complex Pe prove to be purely imaginary. Owing to this, we proceed from the initial expansion by a special conformal mapping, $w = w(Pe)$, to a new expansion, in powers of w, which is convergent for all real Pe. The coefficients of the new series can be computed as easily from the FP equation. After the collision efficiency is calculated as a convergent series in powers of w, the effect of the outer boundary is explored. This technique is also applicable to a variety of convection–diffusion problems, including steady heat or mass transfer to an arbitrary-shaped particle (or a collection of particles) at finite Pe, as shown in Appendix B. For practical solution, $p(r)$ is further expanded into Legendre polynomials, and a conservative, second-order finite-difference scheme with respect to particle separation is used. Special measures are undertaken to provide for sufficient mesh refinement at the collision surface, $r = a_1 + a_2$, and to make the scheme economical at large separations (§2.1). This algorithm appears to be much faster than traditional numerical techniques, especially for $Pe \gg 1$. Another decisive advantage of our method is the analytical dependence upon Pe (via w), whereas traditional approaches require a separate calculation for each Pe.

An analytical continuation of a power expansion, as a method for solving convection–diffusion problems at finite Pe, was first used by Kim & Fan (1984) in their study of the orientation distribution function for axisymmetric non-spherical particles in a shear flow. Their technique was successful for values of Pe not exceeding twice the radius h of convergence of the initial expansion. In our case, Pe/h is quite large, owing to $h \ll 1$ and the high values of Pe considered, and so we found it necessary to develop an alternative technique. The familiar Euler transformation (Van Dyke 1974) is also inappropriate for our problem (see §3.2).

The test calculations are discussed in §4, including a delicate comparison of our convergence-tested solution for $Pe \leqslant O(10^3)$ with the trajectory analyses by Zinchenko (1982) and Zhang & Davis (1991). The local asymptotic structure of the solution for high but finite Pe is also discussed in §4, for the case of no van der Waals force.

Even though our algorithm is capable of providing high accuracy and is far more efficient than the other exact methods attempted, it is computationally slow for $Pe \geqslant O(100)$. For this reason, an approximate solution based on neglecting the transversal diffusion is also considered (§5). The same simplification was used *ad hoc* by Prieve & Ruckenstein (1974), to calculate collision rates for solid spheres of very small size ratio.

In §6, the systematic results are presented for the collision efficiency as a function of the size ratio, the drop-to-medium viscosity ratio, and the Péclet number, for wide ranges of these parameters, with and without unretarded van der Waals forces. The exact results are compared with those from a trajectory analysis (Zhang & Davis 1991), with our approximate solution, and with the so-called additive approximation. The effect of electromagnetic retardation of the van der Waals forces on the collision efficiency is also studied, for a wide range of particle size. All the calculations have been performed on an IBM PC 486.

2. Formulation of the problem

Consider a dilute, locally homogeneous emulsion containing spherical drops of viscosity μ' and density ρ' dispersed in an immiscible fluid of viscosity μ_e and density ρ_e. Both fluids are Newtonian and isothermal, and it is assumed that there are no surfactants or interfacial tension gradients on the drop surfaces. The presence of

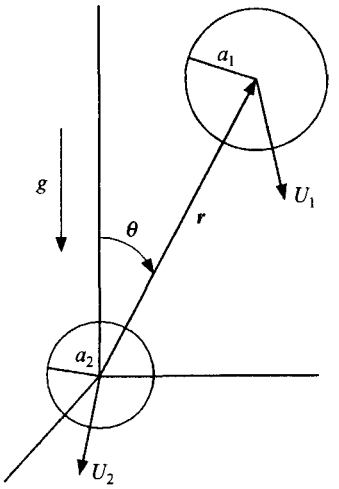

FIGURE 1. Schematic of the coordinate system used for the relative motion of two different-sized drops.

impurities on the drop surfaces gives rise to interfacial tension gradients which cause the drops to behave like rigid spheres; this situation is described by our analysis in the limit $\mu'/\mu_e \to \infty$. For dilute dispersions, the probability of a third drop influencing the relative motion of two interacting drops is small, and so the analysis is restricted to binary interactions of drops with radii a_1 and a_2, as shown in figure 1. The interfacial tension is assumed large enough to keep the drop surfaces spherical, and the particles are sufficiently small so that their inertia is negligible and the quasi-steady Stokes equations hold for the fluid motion inside and outside the drops. The relative drop motion is affected by gravity, Brownian diffusion, and interparticle van der Waals attraction. Only 'rapid' coagulation or coalescence is considered herein, and so repulsive forces are neglected, as discussed by Zhang & Davis (1991).

In the dilute limit, the pair distribution function $p(\boldsymbol{r})$, which is the probability density to find a sphere of radius a_1 centred at $\boldsymbol{r}$ provided that there is a sphere of radius a_2 centred at the origin, satisfies the quasi-steady Fokker–Planck type equation

$$\boldsymbol{\nabla} \cdot (p(\boldsymbol{r})\, \boldsymbol{V}_{12}(\boldsymbol{r})) = 0. \tag{2.1}$$

The relative velocity $\boldsymbol{V}_{12} = \boldsymbol{V}_1 - \boldsymbol{V}_2$ is of the form (Batchelor 1982; Zhang & Davis 1991)

$$\begin{aligned} \boldsymbol{V}_{12}(\boldsymbol{r}) = {} & \boldsymbol{V}_{12}^{(0)} \cdot [\boldsymbol{nn} L(s) + (\boldsymbol{I} - \boldsymbol{nn})\, M(s)] \\ & - \frac{D_{12}^{(0)}}{kT} [\boldsymbol{nn} G(s) + (\boldsymbol{I} - \boldsymbol{nn})\, H(s)] \cdot \boldsymbol{\nabla} \Phi_{12} \\ & - D_{12}^{(0)} [\boldsymbol{nn} G(s) + (\boldsymbol{I} - \boldsymbol{nn})\, H(s)] \cdot \boldsymbol{\nabla} (\ln p(\boldsymbol{r})), \end{aligned} \tag{2.2}$$

where $\boldsymbol{n} = \boldsymbol{r}/r$, $\boldsymbol{I}$ is the unit second-order tensor, and Φ_{12} is the interparticle potential (detailed forms for Φ_{12} are discussed in §6). The relative velocity $\boldsymbol{V}_{12}^{(0)}$ due to gravity for two widely separated drops is given by the Hadamard–Rybczysnki formula (Lamb 1945):

$$\boldsymbol{V}_{12}^{(0)} = \boldsymbol{U}_1^{(0)} - \boldsymbol{U}_2^{(0)} = \frac{2(\hat{\mu}+1)(\rho' - \rho_e)\, a_1^2 (1-\lambda^2)\, \boldsymbol{g}}{3(3\hat{\mu}+2)\, \mu_e}, \tag{2.3}$$

where $\hat{\mu} = \mu'/\mu_e$ is the viscosity ratio, $\lambda = a_2/a_1 < 1$ is the radius ratio, $\boldsymbol{g}$ is the

gravitational acceleration vector, and $U_i^{(0)}$ is the settling velocity of an isolated drop. Similarly, the relative diffusivity due to Brownian motion for two widely separated drops is

$$D_{12}^{(0)} = \frac{kT(\hat{\mu}+1)(1+\lambda^{-1})}{2\pi\mu_e(3\hat{\mu}+2)\,a_1}, \tag{2.4}$$

where k is the Boltzman constant and T is the absolute temperature.

The relative mobility functions for motion along the line of centres (L and G) and motion normal to the line of centres (M and H) describe the effects of hydrodynamic interactions between the two drops. These functions depend on $\hat{\mu}$, λ, and the magnitude s of the dimensionless centre-to-centre vector: $s = 2r/(a_1+a_2)$. Complete information about the hydrodynamic functions L, G, M and H is available from the literature (see §1), including exact bispherical coordinate solutions at arbitrary separations, as well as far-field and near-field asymptotics. In particular, for $s \to \infty$, the standard method of reflections yields

$$\left.\begin{aligned} &G, H = 1 + O(s^{-1}), \\ &M = 1 - \frac{C_M}{s} + O\left(\frac{1}{s^3}\right), \quad L = 1 - \frac{2C_M}{s} + O\left(\frac{1}{s^3}\right), \\ &C_M = \frac{(3\hat{\mu}+2)}{2(\hat{\mu}+1)}\frac{(\lambda^3-1)}{(1+\lambda)(\lambda^2-1)}. \end{aligned}\right\} \tag{2.5}$$

The other relations for the hydrodynamic functions necessary in the present work are outlined in Appendix A.

The three terms on the right-hand side of (2.2) represent the contributions of gravity, interparticle forces, and Brownian diffusion to the drop relative motion, respectively. Their relative importance may be measured by a dimensionless interparticle force parameter, Q_{12}, and the Péclet number:

$$Q_{12} = \frac{\frac{1}{2}(a_1+a_2)\,V_{12}^{(0)}}{AD_{12}^{(0)}/kT}, \quad Pe = \frac{\frac{1}{2}(a_1+a_2)\,V_{12}^{(0)}}{D_{12}^{(0)}}, \tag{2.6}$$

where $V_{12}^{(0)} = |V_{12}^{(0)}|$ and A is the composite Hamaker constant, which is chosen as a measure of the strength of the interparticle forces (see §6). Assuming that the interparticle force acts along the line of centres, we have the following expression for the dimensionless relative velocity $\boldsymbol{u} = \boldsymbol{V}_{12}/V_{12}^{(0)}$ (Zhang & Davis 1991):

$$\begin{aligned} \boldsymbol{u} = &-L(s)\cos\theta\,\boldsymbol{e}_r + M(s)\sin\theta\,\boldsymbol{e}_\theta - \frac{1}{Q_{12}}G\phi'(s)\,\boldsymbol{e}_r \\ &-\frac{1}{Pe}\left[G(s)\frac{\partial(\ln p)}{\partial s}\boldsymbol{e}_r + \frac{H(s)}{s}\frac{\partial}{\partial\theta}(\ln p)\,\boldsymbol{e}_\theta\right], \end{aligned} \tag{2.7}$$

where $\boldsymbol{e}_r$ and $\boldsymbol{e}_\theta$ are unit vectors in the radial and tangential directions in a spherical polar coordinate system (see figure 1), respectively, and $\phi = \Phi_{12}/A$ is the dimensionless interparticle force potential, and $\phi' = \mathrm{d}\phi/\mathrm{d}s$.

The inner boundary condition is

$$p = 0 \quad \text{for } r = a_1 + a_2, \tag{2.8}$$

which results from the assumption that the colliding drops coalesce (or flocculate, in

the case of solid spheres) upon contact. The absence of far-field correlations yields the outer boundary condition

$$p \to 1 \quad \text{for } r \to \infty. \tag{2.9}$$

The collision rate J_{12} is the flux of pairs into the contact surface $r = a_1 + a_2$ and is given by

$$J_{12} = -n_1 n_2 \int_{r \to a_1+a_2} p V_{12} \cdot \boldsymbol{n} \, \mathrm{d}A, \tag{2.10}$$

where n_1 and n_2 are the number of drops at a given time in the size categories characterized by radius a_1 and a_2, respectively, per unit volume of the dispersion. Using (2.1) and the divergence theorem, the integral in (2.10) may be taken over any surface enclosing the contact surface. If the drops are assumed to more independently, without hydrodynamic and interparticle interaction and without Brownian diffusion, the collision rate is given by the classical Smoluchowski relation

$$J_{12}^{(0)} = n_1 n_2 V_{12}^{(0)} \pi (a_1 + a_2)^2. \tag{2.11}$$

The collision efficiency E is defined as

$$E = J_{12}/J_{12}^{(0)}. \tag{2.12}$$

As discussed in §1, only the limiting cases $Pe \ll 1$ and $Pe \gg 1$ have been rigorously considered so far. A more comprehensive numerical solution, valid for arbitrary values of Pe, Q_{12}, and any form of interparticle potential $\phi(s)$, is obtained in the present work. Note that, for a given form of $\phi(s)$ for which the Hamaker constant is the only parameter, the collision efficiency E depends on four dimensionless parameters λ, $\hat{\mu}$, Pe and $\hat{A} \equiv A/kT = Pe/Q_{12}$. Thus, an efficient numerical technique is needed to allow for comprehensive calculations.

3. Method for the exact solution at arbitrary Péclet numbers

3.1. *Discretization*

As the first step, the pair distribution function is expanded into Legendre polynomials, P_n:

$$p(s) = \sum_{n=0}^{\infty} a_n(s) P_n(\cos\theta). \tag{3.1}$$

Legendre polynomials are chosen because the pair distribution function is axisymmetric. It is also convenient to expand the radial probability flux in a similar way:

$$-s^2 p u_r = \frac{1}{Pe} \sum_{n=0}^{\infty} q_n(s) P_n(\cos\theta). \tag{3.2}$$

Substituting (2.7) and (3.1) into (3.2), and using the recurrent properties of Legendre polynomials (Abramowitz & Stegun 1972), yields the relation between $a_n(s)$ and $q_n(s)$:

$$q_n = s^2 G \frac{\mathrm{d}a_n}{\mathrm{d}s} + \hat{A} s^2 G \phi'(s) a_n + Pe\, s^2 L \left[\frac{n}{2n-1} a_{n-1} + \frac{n+1}{2n+3} a_{n+1} \right] \quad \text{for } n \geqslant 0. \tag{3.3}$$

Using (2.7), the FP equation (2.1) can be written as

$$\frac{1}{s^2}\frac{\partial}{\partial s}[s^2 p u_r] + \frac{M}{s \sin\theta}\frac{\partial}{\partial\theta}(p \sin^2\theta) - \frac{H}{Pe\, s^2 \sin\theta}\frac{\partial}{\partial\theta}\left(\sin\theta \frac{\partial p}{\partial\theta}\right) = 0. \tag{3.4}$$

Substituting (3.1) and (3.2) into (3.4), and using again the properties of $P_n(\cos\theta)$, we arrive at the second relation:

$$\frac{dq_n}{ds} = n(n+1)\,Ha_n + Pe\,sMn(n+1)\left[\frac{a_{n-1}}{2n-1} - \frac{a_{n+1}}{2n+3}\right] \quad \text{for } n \geqslant 0. \tag{3.5}$$

The relations (3.3) and (3.5) can be considered as an infinite system of first-order differential equations for $a_n(s)$ and $q_n(s)$. A special transformation of (3.3) and (3.5) is used to considerably reduce the number of nodes of our finite-difference approximation at large separations. First, we note that, for $Pe \neq 0$ and $s \to \infty$, the coefficients a_n with $n \neq 0$ behave like $O(s^{-2})$ and $a_0 = 1 + O(s^{-2})$ (see Appendix C). So, we proceed from $a_n(s)$ to new functions

$$b_n(s) = s^2[a_n(s) - \delta_{n,0}] \tag{3.6}$$

(with δ_{ij} being the Kronecker delta) which are smoother at large separations. More significantly, equation (3.3) shows that all functions $q_n(s)$ with $n \neq 1$ are limited as $s \to \infty$, whereas $q_1(s)$ behaves like $O(s^2)$, which hampers an accurate finite-difference representation at $s \gg 1$. The necessary transformation from $q_n(s)$ to new coefficients $\tilde{q}_n(s)$ is of the form

$$q_n(s) = \tilde{q}_n(s) + \delta_{n,1}\,Pe\,s^2\left(1 - \frac{2C_M}{s}\right), \tag{3.7}$$

with C_M defined in (2.5). The system (3.3) and (3.5), written in the new variables $b_n(s)$ and $\tilde{q}_n(s)$, takes the form

$$\tilde{q}_n = G\frac{db_n}{ds} - \frac{2G}{s}b_n + \hat{A}G\phi'(s)[b_n + \delta_{n,0}s^2] + Pe\,L\left[\frac{n}{2n-1}b_{n-1} + \frac{n+1}{2n+3}b_{n+1}\right] + \delta_{n,1}\,Pe\,s^2\left[L - 1 + \frac{2C_M}{s}\right], \tag{3.8}$$

$$\frac{d\tilde{q}_n}{ds} = \frac{n(n+1)\,Hb_n}{s^2} + \frac{Pe\,Mn(n+1)}{s}\left[\frac{b_{n-1}}{2n-1} - \frac{b_{n+1}}{2n+3}\right] + 2\delta_{n,1}\,Pe\,s\left[M - 1 + \frac{C_M}{s}\right]. \tag{3.9}$$

It follows from (3.8), (3.9), and the asymptotics (2.5) that all $\tilde{q}_n(s)$, as well as $b_n(s)$, approach constant values as $s \to \infty$, and so a relatively few nodes of our finite-difference approximation to (3.8) and (3.9) suffice at large separations. This improvement allows us to considerably increase the number of nodes at the collision surface $s = 2$, which is particularly important for the case of a weak attractive force and high Péclet numbers. Using a monotonically increasing mapping, $s = s(x)$ (with $s(0) = 2$), the system (3.8) and (3.9) can be rewritten in a general form as

$$\frac{db_n}{dx} = \Phi(x, \tilde{q}_n, b_{n-1}, b_{n+1}, Pe), \tag{3.10}$$

$$\frac{d\tilde{q}_n}{dx} = \psi(x, b_n, b_{n-1}, b_{n+1}, Pe). \tag{3.11}$$

A conservative, second-order finite-difference approximation to (3.10)–(3.11) is used on a uniform mesh, $0 = x_0 < x_1 < \ldots < x_I$:

$$db_n/dx \approx (b_n^{i+1} - b_n^i)/\Delta x, \quad d\tilde{q}_n/dx \approx (\tilde{q}_n^{i+1} - \tilde{q}_n^i)/\Delta x, \tag{3.12}$$

$$\tilde{q}_n \approx \tfrac{1}{2}(\tilde{q}_n^i + \tilde{q}_n^{i+1}), \quad b_m \approx \tfrac{1}{2}(b_m^i + b_m^{i+1}), \tag{3.13}$$

where $b_n^i = b_n(s(x_i))$ and $\tilde{q}_n^i = \tilde{q}_n(s(x_i))$. Exact values for the other quantities in (3.10)–(3.11) are evaluated at the middle point, $x_{i+1/2}$, where $0 \leqslant i \leqslant I-1$. It seems difficult to find an optimum form of the mapping $s = s(x)$ at the inner boundary, since the answer would depend on a particular choice of the norm in the solution space, the Péclet number, etc. In our calculations, the best convergence, as $I \to \infty$, for the collision efficiency was achieved, on the average, for the mapping

$$[s(s-2)]^{1/4} = x, \tag{3.14}$$

which has rather restrictive mesh refinement at $s \approx 2$, but is quite economical at large separations.

The inner boundary condition (2.8) takes the form

$$b_n^0 = -4\delta_{n,0}. \tag{3.15}$$

The best choice for the computational outer-boundary condition would be $\mathrm{d}b_n/\mathrm{d}s \approx 0$. However, for high Pe, this condition may violate our method of solution (see §3.2). So, a simpler, stiff boundary condition was used in the present work:

$$b_n^I = 0, \tag{3.16}$$

which distorts the asymptotics $b_n(s) \to \text{const} \neq 0$ only in the vicinity of the outer boundary $s = s_I = s(x_I) \gg 1$. The Galerkin expansion (3.1) is truncated, as usual:

$$b_n^i = 0 \quad \text{for } n > N. \tag{3.17}$$

Once the mapping (3.14) is fixed, the only accuracy-determining program parameters include the number $I+1 \gg 1$ of nodes with respect to particle separation, the maximum order $N \gg 1$ of harmonics included, and the position $s_I \gg 1$ of the outer boundary. In the specific case of very high viscosity ratio $\hat{\mu}$, it is difficult to accurately calculate the asymmetric hydrodynamic functions M and H for very small separations (see Appendix A). For this case, the initial node is chosen slightly different from touching:

$$x_0 = [\xi_0(\xi_0+2)]^{1/4}, \tag{3.18}$$

with $\xi_0 \ll 1$ and $b_n^0 = -(2+\xi_0)^2\delta_{n,0}$ instead of (3.15). For very high $\hat{\mu}$, the van der Waals attraction should be necessarily included; otherwise, the region of small separations would affect the collision efficiency too much, thus invalidating the physical model of undeformable drops (Zinchenko 1982). Owing to this, in our calculations with $\hat{\mu} = 10^4$ and attractive forces present, the limit $\xi_0 \to 0$ was achieved with high accuracy for $\xi_0 = 10^{-2} - 10^{-3}$, where numerical calculations of M and H are still quite reliable.

Once the boundary-value, finite-difference problem (3.10)–(3.17) for b_n^i and $\tilde{q}_n^i$ is solved, the collision efficiency can be found as

$$E = \tilde{q}_0^i/Pe. \tag{3.19}$$

The result is independent of $i \in [0, I]$.

3.2. *The solution of the discretized problem by an analytical continuation*

The traditional semi-implicit scheme for the solution of the finite-difference problem (3.10)–(3.17), with time dependence introduced and the diffusive and van der Waals parts being taken at the new timestep, proved too inefficient for systematic use, especially for $Pe \geqslant O(10^2)$ when an extremely slow convergence to a steady state was observed, even for a maximum allowed timestep. A far more efficient technique was exploited in the present work based on an analytical continuation of the solution into the plane of complex Péclet numbers.

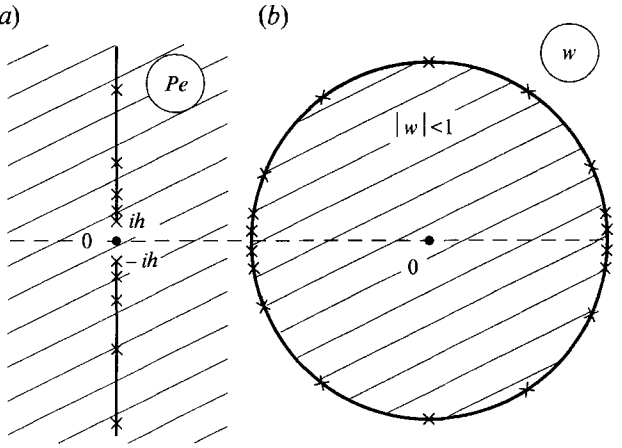

FIGURE 2. Conformal mapping from the Péclet-number plane (*a*) to *w*-plane (*b*). The crosses are the spectrum points.

In dimensionless form, (2.1) can be written as

$$\nabla \cdot (\boldsymbol{D} \cdot \nabla p + \hat{A} G \phi'(s) p \boldsymbol{e}_r) = Pe\, \nabla \cdot (p \boldsymbol{v}), \tag{3.20}$$

where $\boldsymbol{D} = \boldsymbol{nn}G + (\boldsymbol{I} - \boldsymbol{nn})H$ is the dimensionless relative diffusion tensor and $\boldsymbol{v}$ is the convective part of the relative velocity given by the first two terms in (2.7). The solution of the initial problem (2.1), (2.8) and (2.9) cannot be expanded into powers of Pe, since, in the infinite region $2 \leqslant s < \infty$, this is a problem of singular perturbations (see Wang & Wen 1990). However, if the condition $p = 1$ is imposed on any remote, but finite outer boundary, as in (3.16), the power expansion becomes possible. Fixing $\hat{A} = A/kT$, we have

$$p(s) = p_0(s) + Pe\, p_1(s) + \ldots + Pe^{\nu} p_{\nu}(s) + \ldots, \tag{3.21}$$

$$\nabla \cdot (\boldsymbol{D} \cdot \nabla p_{\nu} + \hat{A} G \phi'(s) p_{\nu} \boldsymbol{e}_r) = \nabla \cdot (p_{\nu-1} \boldsymbol{v}) \quad \text{for } \nu \geqslant 0, \tag{3.22}$$

with $p_{-1} \equiv 0$ and appropriate boundary conditions specified for p_{ν}. Consider the spectrum for (3.20), i.e. the set of Péclet numbers in the complex plane for which the problem (3.20), with the boundary conditions $p = 0$ at $s = 2$ and at the outer boundary, has a non-trivial solution $p \not\equiv 0$. Assume that all the spectrum is purely imaginary (see below) and h is the distance from zero to the two nearest spectrum points, $Pe = \pm hi$ (see figure 2*a*). The expansion (3.21) is of little use for calculations, since it is convergent only for $|Pe| < h$, and, necessarily, $h \to 0$ when the position $s = s_I$ of the outer boundary tends to infinity. However, the conformal transformation

$$Pe = \frac{2hw}{1 - w^2} \tag{3.23}$$

maps the plane of Pe with two cuts from $\pm hi$ to ∞ (solid lines in figure 2*a*) onto the unit circle $|w| < 1$. In particular, all the spectrum (crosses in figure 2) is mapped into the circumference $|w| = 1$. Hence, the solution as a function of w is regular inside the circle $|w| < 1$ and can be represented there as a convergent series

$$p(s) = \hat{p}_0(s) + w\hat{p}_1(s) + \ldots + w^{\nu}\hat{p}_{\nu}(s) + \ldots. \tag{3.24}$$

As a result, the convergence of (3.24) is guaranteed for all positive real Péclet numbers, since $0 < w < 1$ for $0 < Pe < \infty$. Starting from (3.24), all the quantities of interest, i.e. the collision rate (2.10), can also be represented as convergent series in powers of w. This is the essence of our method.

From a computational viewpoint, it would be a mistake to try calculating a sufficient number of terms in (3.21) and then re-expand (3.21) into powers of w using (3.23), because of a catastrophic loss of accuracy as ν increases. Instead, the relation (3.23) should be substituted directly into (3.20), and the scheme for determining the successive terms in (3.24) then becomes

$$\nabla\cdot[\boldsymbol{D}\cdot\nabla(\hat{p}_\nu-\hat{p}_{\nu-2})+\hat{A}G\phi'(s)(\hat{p}_\nu-\hat{p}_{\nu-2})\,\boldsymbol{e}_r]=2h\nabla\cdot(\hat{p}_{\nu-1}\,\boldsymbol{v})\quad\text{for }\nu\geqslant 0,\tag{3.25}$$

with $\hat{p}_{-2}=\hat{p}_{-1}=0$ and appropriate boundary conditions specified for $\hat{p}_\nu$. The only difference of (3.25) from (3.22) is that $(\hat{p}_\nu-\hat{p}_{\nu-2})/(2h)$ is calculated first via $\hat{p}_{\nu-1}$ and then used to find $\hat{p}_\nu$. So, an arbitrary number of terms in (3.21) and in (3.24) can be computed, if the left-hand side operator in (3.20) is easily invertible.

The basic question, however, is whether the spectrum for (3.20) lies on the imaginary axis. Remarkably, this property of the spectrum can be analytically proved for (3.20), if $\hat{A}=0$ and $\nabla\cdot\boldsymbol{v}=0$ (see Appendix B), which includes a large number of convection–diffusion problems (but not the present one). Another question is whether the spectrum remains purely imaginary when a Galerkin and/or finite-difference approximation to (3.20) is used. These two questions are resolved as described below.

First, an expansion into powers of Pe is applied to the discrete problem (3.10)–(3.17), resulting in

$$b_n^i=b_{n,0}^i+Pe\,b_{n,1}^i+\ldots+Pe^\nu b_{n,\nu}^i+\ldots,\tag{3.26}$$

$$\tilde{q}_n^i=\tilde{q}_{n,0}^i+Pe\,\tilde{q}_{n,1}^i+\ldots+Pe^\nu\tilde{q}_{n,\nu}^i+\ldots.\tag{3.27}$$

For given ν and n, the finite-difference problem for determining $b_i=b_{n,\nu}^i$ and $\tilde{q}_i=\tilde{q}_{n,\nu}^i$ is of the form

$$\alpha_i b_i+\beta_i b_{i+1}=\tilde{q}_i+\tilde{q}_{i+1}+f_i\qquad\text{for }0\leqslant i\leqslant I-1,\tag{3.28}$$

$$\tilde{q}_{i+1}-\tilde{q}_i=\gamma_i(b_i+b_{i+1})+g_i\quad\text{for }0\leqslant i\leqslant I-1,\tag{3.29}$$

$$b_0=-4\delta_{n,0}\qquad b_I=0,\tag{3.30}$$

where the coefficients α_i, β_i, and γ_i are given, and f_i and g_i are calculated via $b_{n\pm1,\nu-1}^i$ and $b_{n\pm1,\nu-1}^{i+1}$. For every ν and n, taken as parameters, the system (3.28)–(3.30) with a band matrix is solved economically by a Gaussian elimination technique to determine b_i and $\tilde{q}_i$. Namely, each solution of (3.28)–(3.29) satisfying the boundary condition $b_I=0$, also satisfies

$$b_i=Q_i\tilde{q}_i+R_i\quad\text{for }0\leqslant i\leqslant I,\tag{3.31}$$

$$b_{i+1}=L_i b_i+K_i\quad\text{for }0\leqslant i\leqslant I-1,\tag{3.32}$$

where the coefficients Q_i, R_i, L_i and K_i allow recurrent calculation in the order of descending i. The other boundary condition (3.30) is then used, together with (3.31)–(3.32), to successively calculate $b_0,\tilde{q}_0,\ldots,b_I$, and $\tilde{q}_I$.

Obviously, $b_{n,\nu}^i$ and $\tilde{q}_{n,\nu}^i$ are equal to zero for $n\not\equiv\nu\,(\mathrm{mod}\,2)$. In particular, the most important quantity, $\tilde{q}_0^i$ (see (3.19)), is expanded into even powers:

$$\tilde{q}_0^i=q_{0,0}+Pe^2q_{0,2}+Pe^4q_{0,4}+\ldots.\tag{3.33}$$

The analysis of Domb–Sykes ratios (Van Dyke 1974), $q_{0,\nu}/q_{0,\nu+2}$, in several calculations showed that the nearest (to zero) singularity for the expansion (3.33) in the plane of Pe^2 lies on the real negative axis and is a simple pole. The distance h^2 from zero to this singularity is

$$h^2=\lim_{k\to\infty}|q_{0,2k}/q_{0,2k+2}|\tag{3.34}$$

and can be computed to nearly machine double precision using 40–50 terms in (3.33).

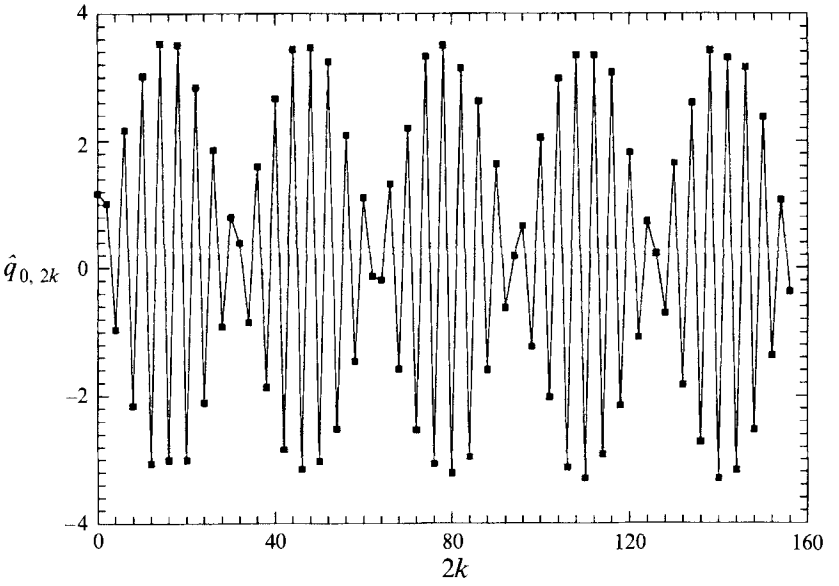

FIGURE 3. Typical behaviour of the Taylor coefficients, $\hat{q}_{0,2k}$. $\lambda = 0.5$, $\hat{\mu} = 2$, $N = I = 50$, $s_I = 10$.

Subtraction of the nearest singularity contribution and the analysis of Domb–Sykes ratios for the remainder of the series (3.33) (see Van Dyke (1974) for the procedure) reveals that the next singularity in the plane of Pe^2 is also real and negative. It is impossible to proceed far with this estimation of the spectrum, because of a rapid loss of accuracy. Instead, our method can be implemented based on the hypothesis that all singularities for (3.33) in the plane of Pe^2 lie on the real negative axis. Namely, the relation (3.23), with $h > 0$ given by (3.34), is substituted into the finite-difference form of (3.10)–(3.11), to directly compute the expansions of b_n^i and $\tilde{q}_n^i$ in powers of w:

$$\tilde{q}_0^i = \hat{q}_{0,0} + w^2\hat{q}_{0,2} + \ldots + w^{2k}\hat{q}_{0,2k} + \ldots . \tag{3.35}$$

Technically, (3.35) is constructed in almost the same manner as (3.33) (cf. (3.22) and (3.25)).

The coefficients $\hat{q}_{0,2k}$ remain of order of unity when $k \to \infty$, as shown in figure 3 for $\hat{A} = 0$ and a rather coarse discretization. This behaviour is typical for all our calculations with various λ, $\hat{\mu}$, $\hat{A}$, N, I and s_I. Thus, (3.35) has always the unit radius of convergence, and the spectrum for (3.20) is, indeed, purely imaginary. Our discretization never violates this property, which may be due to the conservative property of the finite-difference scheme used. However, the spectrum was observed to deviate slightly from the imaginary axis for the case of the soft outer boundary condition $\mathrm{d}b_n/\mathrm{d}s \approx 0$ – which is the reason why (3.16) was preferred in our calculations.

For a given Pe, the expansion (3.35) was found to be much more efficient than the 'time-dependent' approach. Another, and decisive, advantage of our method is the analytical dependence on Pe (via w), and so the solution for a whole set $Pe_1 < \ldots < Pe_m$ of necessary Péclet numbers (with reasonable m) is as efficient as for $Pe = Pe_m$, whereas the time-dependent approach requires a separate calculation for each Pe. Since $w \approx 1$ for $Pe = Pe_m$, a reasonable upper estimate of the tail in (3.35) for all $Pe \leqslant Pe_m$ can be made, replacing $\hat{q}_{0,2k}$ for high k by the average of $|\hat{q}_{0,2k}|$ and summing up the geometric progression in (3.35) with $w = w(Pe_m)$.

Unlike our method based on (3.23), the traditional Euler transformation $Pe^2 = uh^2/(1-u)$ (see Van Dyke 1974) is very unsuitable for this problem. Indeed, the series (3.33) re-expanded in powers of u would be convergent for $|u| < 1$ (and, hence, for all real $Pe > 0$). However, apart from the difficulty of re-expanding, many more terms than used in (3.35) would be required, since $u \simeq 1-h^2/Pe^2$, whereas $w \simeq 1-h/Pe$ for $h/Pe \ll 1$.

It is interesting to note that the radius h of convergence of (3.21) has a universal asymptote $2\pi/s_I$, when the outer boundary $s = s_I$ tends to infinity, independent of λ, $\hat{\mu}$, $\hat{A}$ and $\phi(s)$ (see Appendix C). The behaviour $h \sim s_I^{-1}$ can be understood from the fact that, for $Pe \ll 1$, the expansion (3.21) is expected to diverge when the outer boundary is 'somewhere' in the outer asymptotic region (Wang & Wen 1990), $s \geqslant 0(Pe^{-1})$.

The relation (3.34) yields the optimum h for the best convergence of (3.35). However, any slightly smaller value can be used, with nearly the same efficiency. Thus, high accuracy in determining h from (3.34) is not required.

4. Test calculations

To check the method and the code, consider first a model situation, when particles move and diffuse up to contact without any hydrodynamic and van der Waals interaction, i.e. we set $L \equiv M \equiv G \equiv H \equiv 1$ and $\phi \equiv 0$ for all separations. The problem then simplifies to

$$Pe\frac{\partial p}{\partial z} + \nabla^2 p = 0, \tag{4.1}$$

$$p = 0 \quad \text{for } s = 2, \tag{4.2}$$

$$p \to 1 \quad \text{for } s \to \infty, \tag{4.3}$$

where z is the coordinate in the direction of gravity. We call this the 'Smoluchowski model for finite Péclet number', and it has an analytical series solution (see Appendix C). In table 1, the analytical solution is compared with our numerical solution described in §3, and excellent agreement for the collision efficiency E is generally observed. For small Pe, when p approaches unity very slowly as $s \to \infty$, the agreement can be improved by increasing s_I. In the model calculations for table 1, the mapping $(s-2)^{1/2} = x$ was used.

As a very sensitive test of our code with full hydrodynamic interactions, a comparison was made with the solutions of Zinchenko (1982) and Zhang & Davis (1991) for non-Brownian drops without van der Waals attraction. The numerical results by our code are presented in figure 4 for $30 \leqslant Pe \leqslant 750$. As a convergence check for all data, the program parameters were varied in the range $N = 280$–400, $I = 100$–150, and $s_I = 25$–40. It was found that the relative variation in the collision efficiency does not exceed $O(10^{-4})$. The results appear to be a linear function of $Pe^{-1/2}$ for high Pe, and the extrapolation to $Pe = \infty$ using the last two values of each row, as shown in figure 4, yields $E_{ext} = 0.197$, 0.125, 0.091 and 0.060 for $\hat{\mu} = 0$, 0.5, 1 and 2, respectively, in very good agreement with $E_\infty = 0.202$, 0.127, 0.093 and 0.061 by trajectory analyses (Zinchenko 1982; Zhang & Davis 1991):

$$E_\infty = \exp\left[-2\int_2^\infty \frac{M-L}{sL}\,\mathrm{d}s\right], \tag{4.4}$$

where the subscript ∞ refers to $Pe = \infty$.

The slow approach to E_∞ in figure 4, with an error $O(Pe^{-1/2})$, has a simple physical

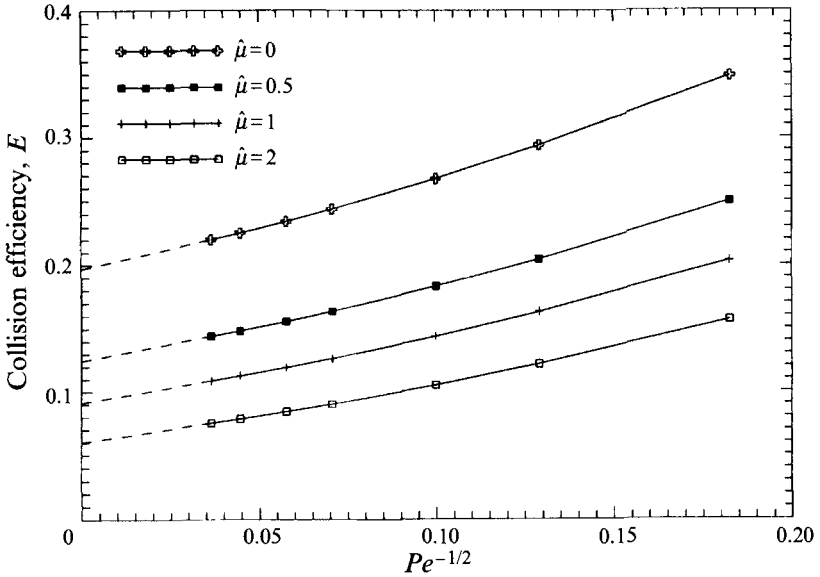

FIGURE 4. Extrapolation of the finite-Péclet-number collision efficiencies to the non-Brownian limit $Pe = \infty$, for $A/kT = 0$, $\lambda = 0.5$.

Pe	0.03	0.1	0.3	1	3	10
Numerical solution						
$I = 100$, $N = 30$, $s_I = 20$	74.24	22.74	8.5316	3.6570	2.1171	1.4619
$I = 200$, $N = 40$, $s_I = 40$	70.54	22.03	8.5126	3.6569	2.1171	1.4619
Analytical solution	68.65	21.94	8.5121	3.6568	2.1170	1.4619

TABLE 1. The collision efficiency for the Smoluchowski model at finite Péclet numbers

explanation. Consider the structure of the solution in a meridian half-section (figure 5) at $Pe = \infty$. The limiting relative trajectory touches the contact surface $s = 2$ at $\theta = \frac{1}{2}\pi$ and separates colliding and non-colliding trajectories. Obviously, $p = 0$ in the 'shadow zone' bounded by the downstream part of the limiting trajectory ($\theta > \frac{1}{2}\pi$), the contact surface, and the symmetry axis. Everywhere outside the shadow zone, $p(s)$ can be found from (2.9) and the Liouville equation: $\nabla \cdot (pv) = 0$. The solution has an isotropic form (Batchelor 1982):

$$p = q(s) = \frac{1}{L}\exp\left[-2\int_s^\infty \frac{(M-L)\,\mathrm{d}s}{Ls}\right]. \tag{4.5}$$

The relation (4.4) follows from (4.5) and (2.7), by integrating the probability flux $-qv_r$ over the upstream part ($0 < \theta < \frac{1}{2}\pi$) of the contact surface $s = 2$. The solution (4.5) is singular at $s \to 2$, as $O((s-2)^{-1/2})$ for $0 < \hat{\mu} < \infty$ and as $O(|\ln(s-2)|)$ for $\hat{\mu} = 0$ (see Appendix A), and it does not satisfy the inner boundary condition $p = 0$, which is corrected for high, but finite Pe by the upstream boundary layer of thickness Pe^{-1}. Similarly, for $1 \ll Pe < \infty$, there exists another boundary layer, along the downstream limiting trajectory, matching $p \approx 0$ (presumably of the order $O(Pe^{-1})$, see §6) in the shadow zone, with $p = q(s)$ outside this region. The thickness of this layer, at $s-2 \sim 1$, is $O(Pe^{-1/2})$, as for any subcharacteristical boundary layer (Cole 1968). (Obviously,

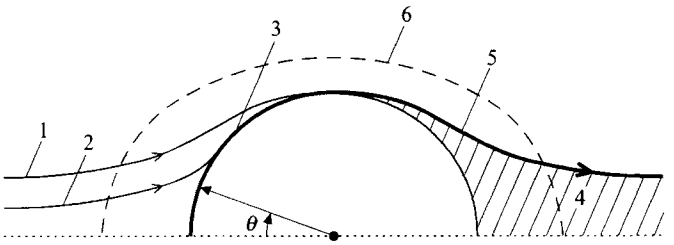

FIGURE 5. On the asymptotic structure of the solution for $Pe \gg 1$ and $A/kT = 0$ in the meridian half-section: 1. upstream part of the limiting trajectory, 2. typical collision trajectory, 3. upstream boundary layer on the contact surface $s = 2$, with $0 < \theta < \frac{1}{2}\pi$, 4. shadow zone, 5. downstream subcharacteristical boundary layer, and 6. control surface.

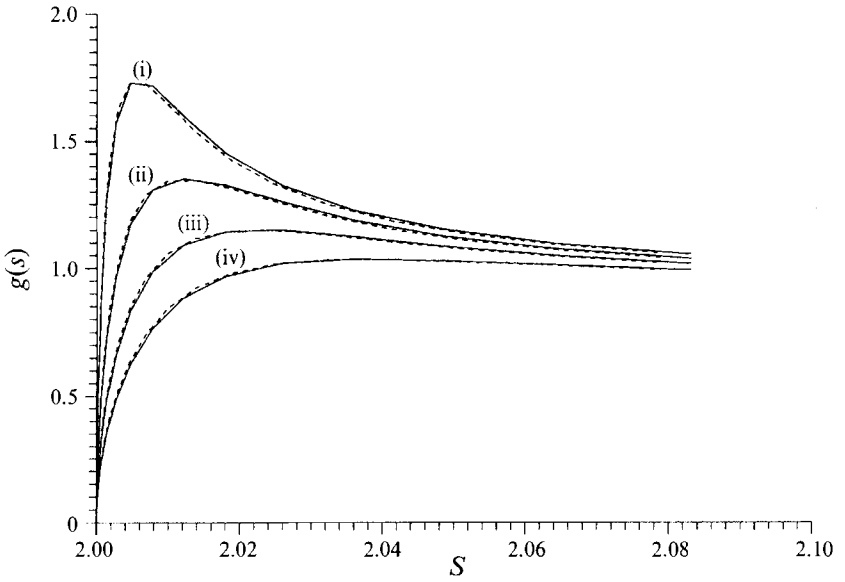

FIGURE 6. Radial distribution function for $\lambda = 0.5$, $\hat{\mu} = 2$, $A/kT = 0$, and different Péclet numbers. Solid lines: $N = 280, I = 150, s_I = 40$; dashed lines: $N = 400, I = 150, s_I = 25$. (i) $Pe = 1000$; (ii) $Pe = 500$; (iii) $Pe = 300$; (iv) $Pe = 200$.

this layer is responsible for a large number of harmonics required in the solution for $Pe \gg 1$.) Owing to the conservation law (2.1), the coalescence rate can be obtained by integrating the probability flux over any closed control surface, well-separated from the enclosed contact surface $s = 2$, as shown in figure 5 by a dashed line. The finite-Péclet-number correction to the probability flux $-p\boldsymbol{u} \cdot \boldsymbol{n}$ is $O(Pe^{-1})$ everywhere on the control surface, except in the boundary layer. In the latter region, $p \sim 1, \boldsymbol{u} \cdot \boldsymbol{n} \sim 1$, and the integration over this portion of the control surface yields the observed $O(Pe^{-1/2})$ correction to the collision efficiency (interestingly, this conclusion is independent of the behaviour of hydrodynamic functions at $s \to 2$, and is valid both for $0 < \hat{\mu} < \infty$ and $\hat{\mu} = 0$). However, we did not attempt to find the slopes of the lines in figure 4 analytically, since it would require an analysis of the solution at the critical point $s = 2$, $\theta = \frac{1}{2}\pi$, to obtain initial conditions for the downstream boundary layer.

Our convergence-tested calculations of the radial distribution function $g(s)$ (i.e. the pair distribution function $p(s)$ averaged over all orientations) in figure 6 are also in agreement with the asymptotic structure of the solution. When the Péclet number is

high, $g(s)$ first tends to be singular as $s \to 2$, and then drops to zero, according to the inner boundary condition. Figure 6 also clearly demonstrates the necessity of mesh refinement in the numerical solution at $s = 2$.

The asymptotic structure of the solution also shows the behaviour of the Fourier coefficients $a_n(s)$ at large distances for $Pe = \infty$. using the orthogonality properties of the Legendre polynomials yields the identity

$$a_n(s) - \delta_{n,o} = \frac{(2n+1)}{4\pi r^2} \int [p(s) - q(s)] P_n(\cos\theta)\, \mathrm{d}A + [q(s) - 1]\, \delta_{n,o}, \tag{4.6}$$

where the integration is taken over a sphere of radius r. The function $p - q$ is non-zero only in the shadow zone of finite thickness at $s \to \infty$, resulting in the $O(s^{-2})$ estimate for the first term of (4.6), whereas the last term is only $O(s^{-6})$ (Batchelor 1982) or zero. These arguments shows a sufficiently fast decay of $a_n(s) - \delta_{n,o}$ at $s \to \infty$ in the non-Brownian limit and help to explain why, even at very high Pe when the wake extends out of the cutoff distance, the latter does not have to be very large for an accurate numerical solution.

5. Approximate approach: parabolization of the Fokker–Planck equation

Even though our algorithm is capable of providing remarkable accuracy and is far more efficient than the other exact methods attempted, it is still too slow for $Pe \gg 1$ to allow for comprehensive calculations. For example, in order to compute the function $E(Pe)$ in the range $0 < Pe < Pe_m$ for $\lambda = 0.5$, $\hat{\mu} = 2$, $N = 200$, $I = 50$ and $s_I = 25$, with a guaranteed convergence in (3.35) to 0.1 % accuracy, it takes about 15 min of CPU time for $Pe_m = 200$ and 54 min for $Pe_m = 500$. So, it is of interest to consider a simpler but approximate approach based on parabolization of the FP equation.

The last term in (3.4), with a factor Pe^{-1}, represents the transversal diffusion and has a zero mean on any sphere $s = \text{const} > 2$, and one can expect a rather small effect of this oscillating term on the solution when $Pe \gg 1$. So, the idea of the approximate approach is to solve, instead of (3.4), the equation

$$\frac{\partial}{\partial s}\left[s^2 p L\mu + \frac{s^2}{Pe} G \frac{\partial p}{\partial s} + \frac{\hat{A} s^2}{Pe} G\phi'(s)\, p\right] = Ms \frac{\partial}{\partial \mu}[p(\mu^2 - 1)], \tag{5.1}$$

with $\mu = \cos\theta$, which is obtained by neglecting the last term in (3.4) and using (2.7). Equation (5.1) is now of parabolic type with respect to μ. Hence, in addition to the boundary conditions (2.8) and (2.9), only the initial condition at $\mu = 1$ is required to start integration to $\mu = -1$, resulting in a quite efficient non-iterative solution. In this particular case, the initial distribution of $p(s)$ is contained in (5.1) on the assumption of the regularity of $p(s, \mu)$ at $\mu = 1$. So, instead of a finite-difference scheme with respect to μ, it is quite natural to expand the solution into powers of $\mu - 1$. All the terms of the expansion can then be found successively from (5.1).

For practical solution, (5.1) is written as a system of two first-order equations, with a special transformation to improve the quality of the finite-difference scheme at large separations (cf. with (3.8)–(3.9)):

$$\frac{\partial q}{\partial s} = \frac{Pe\, M}{s} \frac{\partial}{\partial \mu}[b(\mu^2 - 1)] + 2Pe\, s\mu \left[M - 1 + \frac{C_M}{s}\right], \tag{5.2}$$

$$q = G\frac{\partial b}{\partial s} - \frac{2G}{s} b + \hat{A} G\phi'(s)(b + s^2) + Pe\, \mu \left[Lb + s^2\left(L - 1 + \frac{2C_M}{s}\right)\right], \tag{5.3}$$

where $b = s^2(p-1)$. The finite-difference approximation to (5.2) and (5.3) is similar to that of §3.1 for the system (3.8) and (3.9), with the same mapping (3.14). The finite-difference problems for calculating the successive terms in the power expansions for b and q are solved by the Gaussian elimination technique for band matrices, similar to the procedure used in §3.2. The collision efficiency is then found as

$$E = \frac{1}{2Pe}\int_{-1}^{1} q|_{s=2}\,\mathrm{d}\mu, \tag{5.4}$$

by analytical integration of the power expansion for q.

Unlike the exact method of §3, this approach requires a separate calculation for each Péclet number. Besides, the numerical experiments show that, for very high Pe, the number $I+1$ of finite-difference nodes should be quite large, to ensure the convergence of the power expansion, especially for viscosity ratio $\hat{\mu}$ close to zero and size ratio close to unity. In particular, $Pe \sim 10^3$ may require $I \sim 10^3$ (if $s_I \sim 25$–40). For drops, there should always exist some (very high) critical value Pe^*, so that, for $Pe > Pe^*$, the integration of (5.1) up to $\theta = \pi$ becomes an incorrect Cauchy problem, since at $Pe \to \infty$ the upstream boundary layer exists only for $\theta < \frac{1}{2}\pi$ (see §4). That is the reason why I should be sharply increased at $Pe \approx Pe^*$. This problem does not occur for solid spheres. Nevertheless, this method remains very efficient since, even for $I = 10^3$, the calculation for one Péclet number, $Pe \leqslant 10^3$, takes no more than a few seconds of CPU time, if the hydrodynamic functions are computed beforehand. The validity of this approximation, however, can be checked only by comparison with the exact solution, which is done below.

6. Numerical results for the collision efficiency

6.1. *Calculations without van der Waals forces*

For $Pe \ll 1$, the collision efficiency is $E \simeq C/Pe$, where the coefficient

$$C = \left(\int_2^\infty \frac{\mathrm{d}s}{s^2 G}\right)^{-1} \tag{6.1}$$

was computed by Zhang & Davis (1991) as a function of λ and $\hat{\mu}$. Even though the next term of the asymptotic expansion was not considered in their work, it follows from the analysis of Melik & Fogler (1984*a*) that the knowledge of C allows construction of the two-term asymptotics for $Pe \ll 1$:

$$E \simeq E_A = \frac{C}{Pe} + \frac{C^2}{2}. \tag{6.2}$$

For finite Pe, we found it helpful to plot the ratio E/E_A, which is a relatively weak function of the Péclet number, with the limiting values of unity and $2E_\infty/C^2$ for $Pe \to 0$ and $Pe \to \infty$, respectively. The results are presented in figure 7. To determine E from these data, the values of C from table 2 can be used. The solid lines in figure 7 were calculated by the exact method of §3 with $N = 20$, $I = 400$, and $s_I = 200$ for $0.1 \leqslant Pe \leqslant 2$ and $N = 200$, $I = 100$, and $s_I = 25$ for $2 \leqslant Pe \leqslant 200$, and are convergence-tested. All the solid lines approach unity, as $Pe \to 0$, in agreement with (6.2). The dashed lines represent the convergence-tested parabolized approximation (PA) of §5, extended up to $Pe \sim 10^3$. This approximation appears to be excellent for $Pe \gg 1$ and is practically indistinguishable from the exact solution even for $Pe \sim 5$. As follows from the

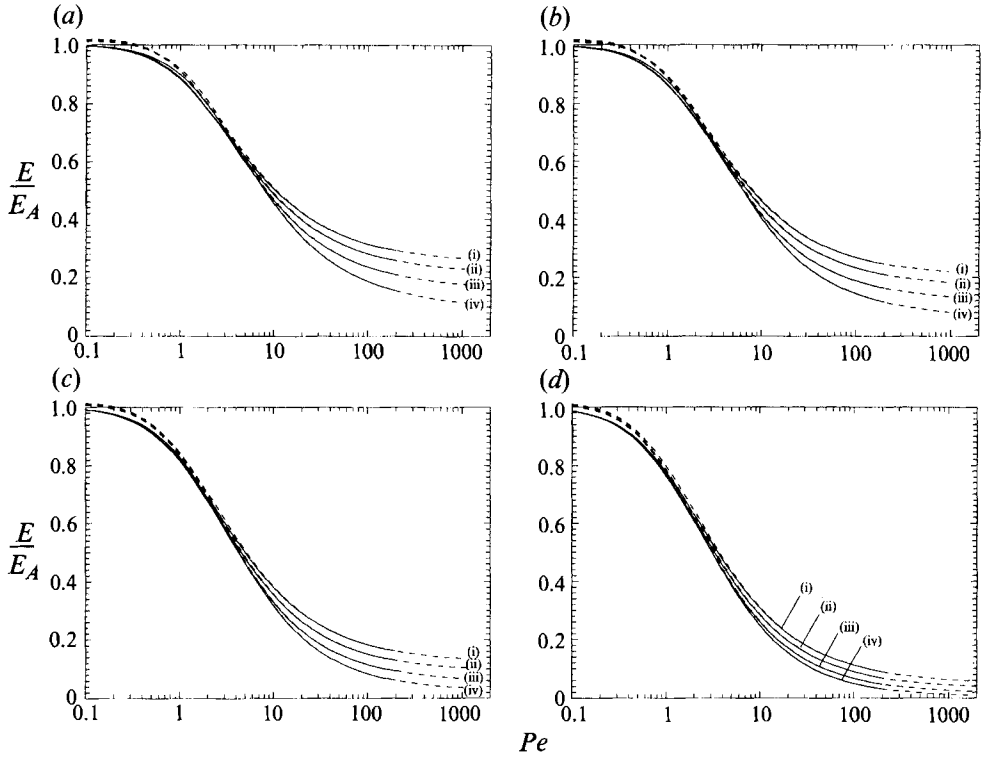

FIGURE 7. Normalized collision efficiency as a function of Péclet number, for drops without van der Waals attraction and having radius ratios (*a*) $\lambda = 0.9$, (*b*) $\lambda = 0.5$, (*c*) $\lambda = 0.25$, and (*d*) $\gamma = 0.10$. The solid lines are from the exact solution, and the dashed lines are from the parabolized Fokker–Planck equation. (i) $\hat{\mu} = 0$; (ii) $\hat{\mu} = 0.5$; (iii) $\hat{\mu} = 2$; (iv) $\hat{\mu} = 10$.

$\hat{\mu}$	$\lambda = 0.1$	0.15	0.25	0.35	0.5	0.75	0.9
0	1.712	1.636	1.531	1.463	1.401	1.356	1.347
0.25	1.653	1.566	1.449	1.375	1.308	1.259	1.250
0.5	1.609	1.514	1.389	1.311	1.242	1.192	1.182
1	1.545	1.440	1.305	1.223	1.151	1.099	1.090
2	1.465	1.349	1.204	1.118	1.044	0.992	0.983
5	1.348	1.219	1.064	0.976	0.902	0.851	0.842
10	1.262	1.125	0.965	0.878	0.806	0.757	0.748

TABLE 2. Values of C in (6.1)

asymptotic structure of the solution at $Pe \gg 1$ (§4) for $s-2 \sim 1$, the last term in (3.4), with zero mean on a sphere of radius s, is only of order of unity in the thin downstream boundary layer and is of order of Pe^{-2} outside this region. Thus, on average, this term is expected to produce little effect. As $s \to 2$, this term seems also insignificant, since the downstream boundary layer approaches the contact surface along the θ-direction. These are possible reasons for the success of PA at moderately high Pe. In the other limit, $Pe \to 0$, the exact solution is independent of θ and is also contained in (5.1). These arguments help to explain why, quite unexpectedly, PA appears to be a very good approximation for all Péclet numbers and size and viscosity ratios, with an error not exceeding 2–3% in any case.

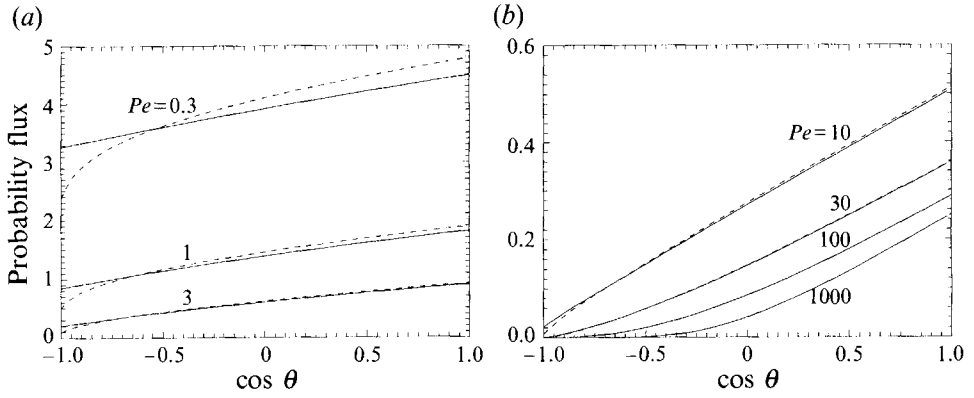

FIGURE 8. Probability flux onto the contact surface, as a function of $\cos\theta$, for drops without van der Waals attraction for (*a*) small and (*b*) large Péclet numbers. The solid lines are from the exact solution, and the dashed lines are from the parabolized Fokker–Planck equation. $\lambda = 0.5$, $\hat{\mu} = 2$.

Even less obvious is whether PA can properly predict local quantities. Figure 8 presents the convergence-tested results for the probability flux,

$$-\lim s^2 p u_r \quad (s \to 2), \tag{6.3}$$

on the contact surface, as a function of $\cos\theta$. Again, PA (dashed lines) is very close to the exact solution for $Pe \geqslant 10$. In particular, a very small local flux from the shadow zone onto the downstream portion of the contact surface ($\cos\theta < 0$) for $Pe \gg 1$, with plausible scaling Pe^{-1}, is properly predicted by PA.

In contrast to PA, it is also interesting to consider another approximation based on the old idea of additivity. This approximation $E \approx C/Pe + E_\infty$ assumes that the collision rates in the limits of strong ($Pe \to 0$) and weak ($Pe \to \infty$) Brownian motion can be simply added, to cover the range of intermediate Péclet numbers. This *ad hoc* approximation has no physical background and can be considered, at best, as an interpolation between the two limits. More importantly, the comparison with the exact calculations, though not shown in figure 7, reveals considerable underestimation of the collision efficiency by the additive approximation for intermediate values of Pe. In case of $\lambda = 0.9$, the maximum error varies from 31 % (for $\hat{\mu} = 0$) to 47 % (for $\hat{\mu} = 10$). For the other values of $\lambda = 0.5$, 0.25 and 0.1, these figures are 34–49 %, 41–54 % and 54–61 %, respectively. One reason for the lack of success of the additive approximation is the improper correction $O(Pe^{-1})$, instead of $O(Pe^{-1/2})$, at $Pe \gg 1$ (see §4).

The ratio E/E_A is only a weak function of λ and $\hat{\mu}$. Thus, figure 7, along with the values of C from table 2, provide a representative description of the collision efficiency for drops with no van der Waals attraction in the range $0.1 \leqslant \lambda \leqslant 1$, with $\hat{\mu} \leqslant 10$.

6.2. *Collision efficiency with van der Waals forces*

The calculations have been also performed for drops and solid spheres with unretarded attractive potential (Hamaker 1937):

$$\Phi_{12} = -\tfrac{1}{6}A\left\{\frac{8\lambda}{(s^2-4)(1+\lambda)^2} + \frac{8\lambda}{s^2(\lambda+1)^2-4(1-\lambda)^2} + \ln\left[\frac{(s^2-4)(1+\lambda)^2}{s^2(1+\lambda)^2-4(1-\lambda)^2}\right]\right\}, \tag{6.4}$$

where A is the composite Hamaker constant. The collision efficiency E now depends

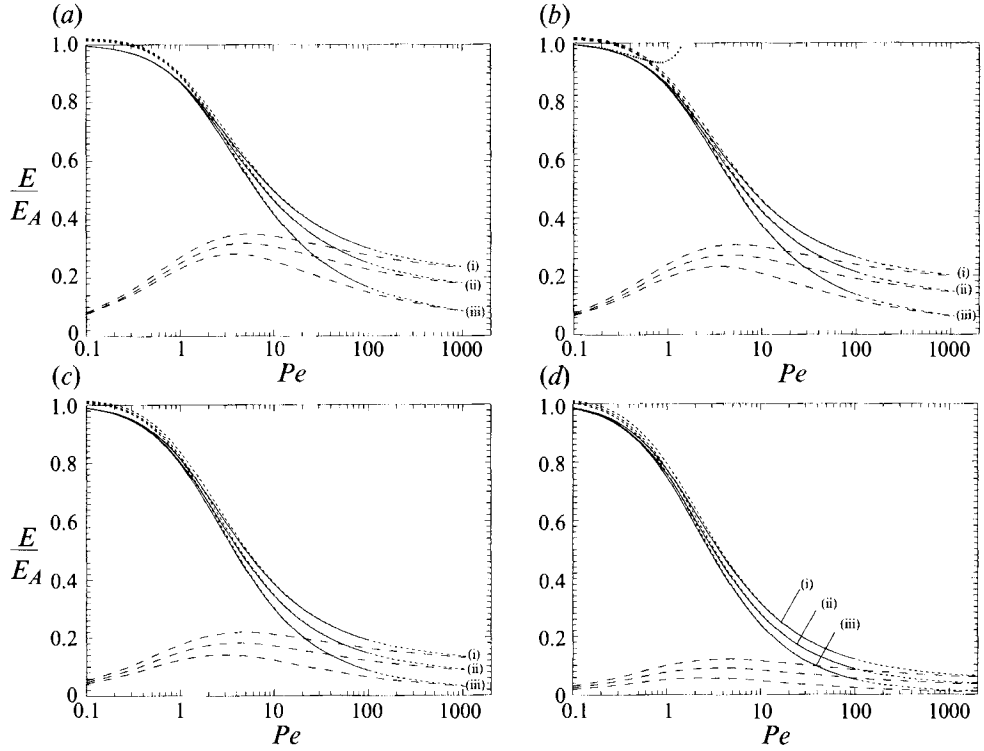

FIGURE 9. Normalized collision efficiency as a function of Péclet number, for drops with unretarded van der Waals attraction and having radius ratios (*a*) $\lambda = 0.9$, (*b*) $\lambda = 0.5$, (*c*) $\lambda = 0.25$, and (*d*) $\lambda = 0.10$. $A/kT = 1.25$. The solid lines are from the exact solution, the short-dashed lines are from the parabolized Fokker–Planck equation, and the long-dashed lines are from the trajectory analysis of Zhang & Davis (1991). The dotted line in (*b*) is from the asymptotic theory of Wang & Wen (1990), equation (6.6). (i) $\hat{\mu} = 0$, (ii) $\hat{\mu} = 1$, (iii) $\hat{\mu} = 10^4$.

$\hat{\mu}$	$\lambda = 0.1$	0.15	0.25	0.35	0.5	0.75	0.9
0	1.790	1.736	1.660	1.609	1.561	1.526	1.519
0.5	1.722	1.655	1.562	1.503	1.447	1.406	1.398
1	1.681	1.607	1.507	1.443	1.384	1.340	1.332
2	1.635	1.554	1.446	1.377	1.315	1.269	1.260
10	1.552	1.458	1.337	1.262	1.196	1.147	1.137
10^4	1.512	1.413	1.286	1.209	1.141	1.091	1.082

TABLE 3. Values of C in (6.5), for unretarded Hamaker Potential (6.4) with $A/kT = 1.25$

on four dimensionless parameters λ, μ, Pe, and A/kT. A typical value $A/kT = 1.25$ was chosen. For $Pe \ll 1$, the asymptotic formula (6.2) holds, with the coefficient

$$C = \left[\int_2^\infty \frac{\exp(\Phi_{12}(s)/kT)}{s^2 G(s)}\,\mathrm{d}s\right]^{-1} \tag{6.5}$$

computed by Zhang & Davis (1991) for several values of the parameters. For the purposes of the present work, the values of C are also given in table 3. The ratios E/E_A are plotted in figure 9. These results can be used along with the data from table 3 to calculate the collision efficiency E. The case $\hat{\mu} = 10^4$ practically corresponds to solid spheres, which are allowed to come into contact due to van der Waals attraction.

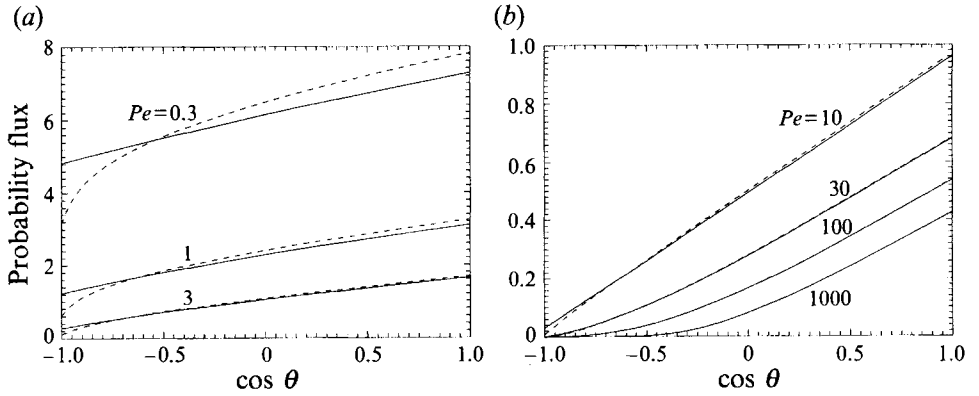

FIGURE 10. Probability flux onto the contact surface, as a function of $\cos\theta$, for drops with unretarded van der Waals attraction at (*a*) small and (*b*) large Péclet numbers. The solid lines are from the exact solution, and the dashed lines are from the parabolized Fokker–Planck equation. $\lambda = 0.25$, $\hat{\mu} = 0.5$, $A/kT = 1.25$.

As for drops without interparticle forces, the parabolized approximation (short-dashed lines in figure 9) is surprisingly very close to the exact solution (solid lines) for all Pe, λ, and $\hat{\mu}$. The two solutions are practically indistinguishable for $Pe \geqslant O(10)$, both for the collision efficiency (figure 9) and for the local probability flux onto the contact surface (figure 10).

The long-dashed lines in figure 9 are from a trajectory analysis, with Brownian diffusion neglected. The dependence on the Péclet number is only due to the interparticle force term in (2.7), with $1/Q_{12} = Pe^{-1}\,A/kT$. To obtain these results, the same method used in Zhang & Davis (1991) was employed, with backward integration to calculate the limiting trajectory. As expected, the trajectory analysis agrees with the exact calculations for $Pe \to \infty$. However, the difference becomes small only for quite large Péclet numbers $Pe \geqslant O(10^2)$.

A comparison is also possible between our calculations for $\lambda = 0.5$ and $\hat{\mu} = 10^4$ and the asymptotic theory of Wang & Wen (1990) for solid spheres. According to their work, for $\lambda = 0.5$, $\hat{\mu} = \infty$, $A/kT = 1.25$, and $Pe \ll 1$,

$$E \simeq 1.14(1 + 0.57\,Pe + 0.253\,Pe^2 \ln Pe - 0.097\,Pe^2)/Pe. \tag{6.6}$$

The ratio E/E_A, where E is given by (6.6) and E_A is the two-term asymptotics (6.2), is plotted in figure 9(*b*) (the dotted line). An excellent agreement with our calculations (the solid line for $\hat{\mu} = 10^4$) is observed when $Pe \ll 1$, but, unfortunately, the range of validity of the asymptotic theory is rather narrow.

Interestingly, the presence of the unretarded van der Waals attraction makes the additive approximation more acceptable, especially for size ratios close to unity, although this approximation still underestimates the collision efficiency. In case of $\lambda = 0.9$, the maximum error of this approximation $E \approx C/Pe + E_T$ (where E_T is the result by a trajectory analysis, see above) varies from 8 % (for $\hat{\mu} = 0$) to 1 % (for $\hat{\mu} = 10^4$). For the other values of $\lambda = 0.5$, 0.25 and 0.1, the corresponding errors are 11–5 %, 18–15 %, and 31–33 %, respectively. So, it is still unreliable to use this approximation for very different size ratios. It should be also noted that, in the presence of the van der Waals force, the additive approximation becomes a numerical method, since the calculation of E_T needs a trajectory integration for each Pe. For this reason, a simple and much more accurate numerical method, based on PA, is preferred.

The Hamaker form (6.4), although frequently used in collision rate calculations,

neglects electromagnetic retardation and is valid only for separations between the drops less than the London wavelength λ_L, which is typically of order 0.1 μm. In principle, the retarded van der Waals potential, valid at arbitrary separations, can be rigorously obtained by Lifshitz theory, but the calculations are complicated (Langbein 1974) and require dielectric data which are specific for each system and not always easily available. In the pairwise approximation, which is unlikely to introduce a large error, the retarded potential was obtained by Clayfield, Lumb & Mackey (1971) by an exact integration of the van der Waals energy between the two atoms, separated by a distance ρ:

$$v = -\frac{\beta}{\rho^6} f(p), \tag{6.7}$$

where $p = 2\pi\rho/\lambda_L$, $\beta = A/(\pi^2 q^2 kT)$, and q is the number density of atoms. The Casimir–Polder approximation for $f(p)$, used by Clayfield *et al.* (1971), has different analytical expressions for $p < 3$ and $p > 3$, resulting, unfortunately, in extremely cumbersome formulae for the total sphere–sphere interaction, especially when differentiation is needed to obtain the force. We believe that, instead of switching between different analytical expressions for $f(p)$, a more attractive approach is to integrate the Shenkel & Kitchener (1960) approximation:

$$f(p) = \frac{2.45}{p} - \frac{2.17}{p^2} + \frac{0.59}{p^3}, \tag{6.8}$$

accurate in the wide region $p > 0.5$. The corresponding formulae (used in the present work) are given in Appendix D and are applicable if $p_0 = 2\pi(s-2)/\nu > 0.5$, with $\nu = 2\lambda_L/(a_1+a_2)$. For $a_i > \lambda_L$ (the only case considered in the present work), the condition $p_o > 0.5$ breaks down only in the geometrically simple region $s-2 \ll 1$, and so in this case the near-field approximation of Ho & Higuchi (1968),

$$\Phi_{12} = -\frac{A}{3(s-2)} \frac{\lambda}{(1+\lambda)^2} \frac{1}{(1+1.769p_o)}, \tag{6.9}$$

is used.

With allowance for retardation, E depends on five dimensionless parameters: λ, $\hat{\mu}$, Pe, A/kT and ν, which complicates a full analysis. Instead, we have chosen typical hydrosol dispersion parameters (Zhang & Davis 1991): $g = 981$ cm s^{-2}, $|\rho' - \rho_e| = 0.1$ g cm^{-3}, $A/kT = 1.25$, $\hat{\mu} = 1$, $\lambda_L = 0.1$ μm, and studied the collision efficiency E versus the radius a_1 of the larger drop for $\lambda = 0.5$. For this system, the Péclet number is $Pe = 0.19\,a_1^4$, where a_1 is in μm. The exact method of §3 becomes more expensive to apply in this case, since the potential $\phi(s)$ in (3.20) depends on Pe via ν, and so the expansion in powers of w should be done anew for each Péclet number, taking ν as a parameter. However, our calculations have comprehensively demonstrated the success of the parabolized approximation for drops with and without unretarded attractions, and so, in the intermediate case of a retarded van der Waals force, the PA is used with confidence, instead of the exact solution. The calculations are presented in figure 11; to avoid logarithmic scales, the results for small and large drop sizes are given separately. The retarded force increases the collision efficiency by no more than 16%. Hence, neglecting the interparticle force may be a reasonable approximation, especially considering the difficulties of reliable calculation of van der Waals attractions. On the other hand, figure 11 shows that the neglect of retardation overestimates the effect of the attractive force, approximately by a factor of 2. Of course, these conclusions have been drawn for $\hat{\mu} = O(1)$ and $A/kT = O(1)$. For high viscosity ratio $\hat{\mu}$, van der Waals

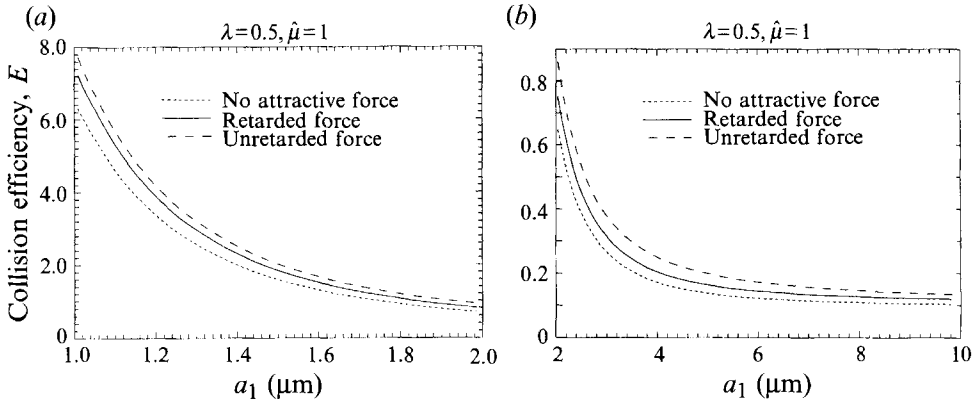

FIGURE 11. The effect of the van der Waals force on the collision efficiency of typical hydrosol drops versus the radius of the larger drop for (*a*) small and (*b*) large drops, with $\Delta\rho = 0.1$ g cm^{-3}, $A/kT = 1.25$, and $\lambda_L = 0.1$ μm. $\lambda = 0.5$, $\hat{\mu} = 1$.

attraction becomes of vital importance (being the only reason for collision of solid spheres), while the effect of retardation is negligible for sufficiently small A/kT (Zhang & Davis 1991).

7. Concluding remarks

Gravity-induced coalescence of spherical drops in a dilute system was considered, with allowance for Brownian motion, internal circulation and van der Waals attraction. As the physical limitations of the present study, we assumed inertia and droplet deformation negligible. For drop radii less than 50 μm, these conditions are usually met, as discussed in detail by Zhang & Davis (1991). An efficient method was developed for the numerical solution of the full Fokker–Planck equation for the pair distribution function at arbitrary Péclet numbers. The method is based on an analytical continuation into the plane of complex Péclet numbers *Pe* (after the boundary condition at infinity has been transferred to some remote, but finite, computational boundary) and on a special conformal mapping, to represent the solution as power series convergent for all real *Pe*. The developed technique is expected to apply to a variety of two- and three-dimensional convection–diffusion problems at arbitrary Péclet numbers.

Using this method, the extensive calculations are presented for the collision efficiency, as a function of size ratio, particle-to-medium viscosity ratio, and the Péclet number, both with and without unretarded van der Waals forces. For typical hydrosols, the effect of Brownian motion on the collision efficiency is pronounced, if $Pe \leqslant O(100)$. In particular, for $Pe \sim 10$, a deterministic trajectory analysis may typically underestimate the collision efficiency by a factor of 2. For drops without van der Waals forces, it was found, both analytically and numerically, that the finite-Péclet-number correction to the collision efficiency is of the order $Pe^{-1/2}$, when $Pe \gg 1$. Excellent agreement was observed between our numerical solution for finite *Pe* and the limiting cases $Pe \ll 1$ and $Pe \gg 1$ studied before.

A parabolic approximate solution (PA) was also considered, based on neglecting the transversal diffusion (along the θ-direction). This parabolization of the Fokker–Planck equation results in a very fast and simple method and yields remarkable accuracy, with an error not exceeding 2–3%. Moreover, this approximation becomes practically

indistinguishable from the exact solution for $Pe \geqslant 5$. The success of PA may be due, in part, to radial symmetry of the interparticle potentials considered. We conclude that PA can be always recommended as a practical method for calculating the gravity-induced collision efficiency for arbitrary size ratio λ, particle-to-medium viscosity ratio $\hat{\mu}$, any form of the van der Waals attractive potential (with or without retardation) and $Pe \leqslant O(10^3)$. The use of PA is particularly helpful for $Pe \geqslant O(10^2)$, when the exact solution becomes slow. For $Pe > 1000$–2000, the solution by PA may be inapplicable, owing to divergence of the power expansion (see §5). However, a trajectory analysis quite suffices for this region.

In contrast to PA, the *ad hoc* additive approximation was found to provide an acceptable accuracy only for particles of close radii with sufficiently strong van der Waals attraction. In the other cases, this approximation is rather poor; in particular, for drops without attractive forces, a maximum error of about 60% was observed.

We also studied the effect of van der Waals attractions on the collision efficiency. For typical emulsion drops of 1–10 μm size, with $\hat{\mu} \sim 1$, $A/kT \sim 1$ and $\lambda = 0.5$, the unretarded force increases the collision efficiency by about 30%. When retardation is taken into account, the increase due to the interparticle force becomes approximately half as much. Hence, for $\hat{\mu} \leqslant O(1)$ and $A/kT \leqslant O(1)$, the neglect of van der Waals attraction may be a reasonable approximation, when dielectric data for rigorous calculation of the molecular force are unavailable.

Our method for the exact solution of the Fokker–Planck equation at arbitrary Péclet numbers is expected to apply to the other problems, such as drop coalescence in shear flows, when the idea of the approximate solution through parabolization fails owing to the complicated nature of relative trajectories.

This work was supported by NSF grant CTS-8914236, NASA grants NAG3-1277 and NAG3-1389, and by a grant from the National Research Council through its Cooperation in Applied Science and Technology Program.

Appendix A. On the calculations of two–drop hydrodynamic functions

The hydrodynamic forces $\boldsymbol{F}_1$ and $\boldsymbol{F}_2$ exerted on the two drops moving with the velocities $\boldsymbol{V}_1$ and $\boldsymbol{V}_2$ in a quiescent liquid can be written as (Zinchenko 1982)

$$\boldsymbol{F}_1 = -6\pi\mu_e a_1[A_{11}(\boldsymbol{V}_1 - \boldsymbol{V}_2)^{\parallel} + A_{12}\,\boldsymbol{V}_2^{\parallel} + T_{11}(\boldsymbol{V}_1 - \boldsymbol{V}_2)^{\perp} + T_{12}\,\boldsymbol{V}_2^{\perp}], \tag{A 1}$$

$$\boldsymbol{F}_2 = -6\pi\mu_e a_2[A_{21}(\boldsymbol{V}_2 - \boldsymbol{V}_1)^{\parallel} + A_{22}\,\boldsymbol{V}_2^{\parallel} + T_{21}(\boldsymbol{V}_2 - \boldsymbol{V}_1)^{\perp} + T_{22}\,\boldsymbol{V}_2^{\perp}], \tag{A 2}$$

where the indices $\parallel$ and $\perp$ denote the vector components along and normal to the line of centres, respectively. The exact reciprocity relations hold for the resistance coefficients A_{ij} and T_{ij}:

$$A_{11} - \lambda A_{21} = A_{12}, \quad T_{11} - \lambda T_{21} = T_{12}. \tag{A 3}$$

Equating $-\boldsymbol{F}_1$ and $-\boldsymbol{F}_2$ to external or thermodynamic forces and using the relation (2.2), one can express the necessary functions L, M, G, H via A_{ij} and T_{ij},

$$L = \frac{(\hat{\mu} + \frac{2}{3})}{(\hat{\mu}+1)(1-\lambda^2)} \frac{(A_{22} - \lambda^2 A_{12})}{(A_{11}A_{22} + A_{12}A_{21})}, \tag{A 4}$$

$$G = \frac{(\hat{\mu} + \frac{2}{3})}{(\hat{\mu}+1)(1+\lambda)} \frac{(A_{12} + \lambda A_{22})}{(A_{11}A_{22} + A_{21}A_{12})}. \tag{A 5}$$

The same relations hold for M and H, respectively, with A_{ij} replaced by T_{ij}. The bispherical coordinate solutions for the axisymmetrical problem are well known

(Rushton & Davies 1973; Haber, Hetsroni & Solan 1973) and, in principle, allow calculation of Λ_{ij} as infinite series at arbitrary separations. In the present calculations, we used a version of bispherical coordinate formalism (Wang, Zinchenko & Davis 1994) with a quite simple algorithm and high accuracy for very small gaps. To calculate the transversal resistance coefficients T_{ij}, and the functions M and H, a more complicated bispherical coordinate solution and the algorithm of Zinchenko (1980) were used.

The convergence of these solutions is slow for very small separations, and so a significant improvement in the efficiency of calculations is achieved by using near-field asymptotics. When $\xi = s-2 \to 0$, the coefficients Λ_{12} and Λ_{22} can be replaced by their finite limiting values Λ_{12}^t and Λ_{22}^t for two touching spheres. For the singular coefficient Λ_{11}, the asymptotics of Zinchenko (1982) hold:

$$\Lambda_{11} \simeq \frac{\pi^2 \hat{\mu} \lambda^{3/2}}{8(1+\lambda)^2 \xi^{1/2}} - \frac{\lambda(3-\hat{\mu}^2)}{9(1+\lambda)} \ln\left[\frac{\xi(1+\lambda)}{2}\right] + c_o, \tag{A 6}$$

where the parameter c_o depends on λ and $\hat{\mu}$. Instead of using cumbersome integral representations for $\Lambda_{12}^t, \Lambda_{22}^t$ (Reed & Morrison 1974) and for c_o (Zinchenko 1982), a more practical method is to estimate these quantities with a sufficient accuracy from the bispherical coordinate solution for several very small separations (with c_o being estimated as the difference between the exact value of Λ_{11} and the sum of the first two terms on the right-hand side of (A 6)). On doing so, we obtain near-field representations for L and G, using (A 4)–(A 5).

The asymptotics (A 6) are not uniformly valid when $\hat{\mu} \to \infty$, i.e. for high viscosity ratio, the range of separations where (A 6) is applicable becomes too small. However, for $\hat{\mu} \gg 1$ and $\xi \ll 1$, a different asymptotic form can be used:

$$\Lambda_{11} \simeq \frac{2\lambda^2}{(1+\lambda)^3} \frac{f(m)}{\xi}, \quad \text{where } m = \frac{1}{\hat{\mu}(1+\lambda)} \left(\frac{2\lambda}{\xi}\right)^{1/2}. \tag{A 7}$$

The function $f(m)$ was calculated numerically by Davies *et al.* (1989) and an accurate Padé-approximate was found:

$$f(m) = \frac{1+0.402\,m}{1+1.711\,m+0.461\,m^2}. \tag{A 8}$$

Unlike (A 6), the asymptotics (A 7) enables the solid-sphere limit $m \to 0$. On the other hand, it can be shown that, when $m \to \infty$, the asymptotics (A 7) matches (A 6) both in the leading term and in the part of the logarithmic term proportional to $\hat{\mu}^2$, provided that $f(m)$ is calculated exactly. A reasonable criterion, for a given $\hat{\mu} \gg 1$, to select between the two asymptotic forms (A 6) and (A 7) is to compare the exact values of L and G with the near-field approximations based either on (A 6) or on (A 7) for a sequence of small separations and choose the form which yields the prescribed accuracy for a wider range of separations.

For asymmetric motion, the coefficients T_{ij} approach their finite limiting values for touching with an error $O(\xi)$ (Zinchenko 1980); thus, for $\xi \ll 1$, a linear extrapolation of M and H can be used, to considerably increase the efficiency of calculations, as in Zhang & Davis (1991). The idea of linear extrapolation fails at very high viscosity ratio $\hat{\mu}$, since, for solid spheres, $M(\xi)$ and $H(\xi)$ approach $M(0)$, $H(0)$ with an error $O(|\ln \xi|^{-1})$ (Batchelor 1976). In our calculations with high values of $\hat{\mu}$, this difficulty was bypassed owing to van der Waals forces, which allowed us to avoid the calculation of hydrodynamic functions at very small separations (see §3.1).

Appendix B. On the spectrum for convection–diffusion problems

Consider a general boundary-value problem for the equation

$$\nabla \cdot (\boldsymbol{D}(\boldsymbol{r}) \cdot \nabla p) = Pe\, \nabla \cdot (p\boldsymbol{v}(\boldsymbol{r})) + f(\boldsymbol{r}) \tag{B 1}$$

in a finite domain V with the boundary $\partial V = \partial V_1 \cup \partial V_2$. The symmetric tensor $\boldsymbol{D}(\boldsymbol{r})$ and the velocity field $\boldsymbol{v}(\boldsymbol{r})$ are assumed to satisfy

$$\boldsymbol{a} \cdot \boldsymbol{D} \cdot \boldsymbol{a} > 0 \quad \text{for } \boldsymbol{a} \neq 0, \tag{B 2}$$

$$\nabla \cdot \boldsymbol{v} = 0 \quad \text{for } \boldsymbol{r} \in V. \tag{B 3}$$

The right-hand side function $f(\boldsymbol{r})$ is assumed given. The boundary conditions for $p(\boldsymbol{r})$ are assumed to be of the first kind on ∂V_1 and of the third one on ∂V_2, i.e.

$$p = \phi \quad \text{for } \boldsymbol{r} \in \partial V_1, \tag{B 4}$$

$$\alpha p + \boldsymbol{n} \cdot \boldsymbol{D} \cdot \nabla p = g \quad \text{for } \boldsymbol{r} \in \partial V_2, \tag{B 5}$$

where the scalar functions $\alpha(\boldsymbol{r}) \geqslant 0$, $\phi(\boldsymbol{r})$, and $g(\boldsymbol{r})$ are given, and $\boldsymbol{n}$ is the outward normal to V. The velocity flux is assumed to vanish on ∂V_2,

$$\boldsymbol{v} \cdot \boldsymbol{n} = 0 \quad \text{for } \boldsymbol{r} \in \partial V_2. \tag{B 6}$$

Consider the spectrum for the problem (B 1), (B 4)–(B 5), i.e. the set of Péclet numbers Pe in the complex plane, for which the corresponding homogeneous spectral problem (i.e. with $f = \phi = g = 0$) has a non-trivial solution $p \neq 0$. It is remarkable that all the spectral values of Pe lie on the imaginary axis.

As proof, consider a linear space $\mathscr{F}$ of complex-valued functions $p(\boldsymbol{r})$ satisfying the homogeneous boundary conditions (B 4)–(B 5), and the operator A in $\mathscr{F}$: $p_2 = Ap_1$, if

$$\nabla \cdot (\boldsymbol{D} \cdot \nabla p_2) = \nabla \cdot (p_1 \boldsymbol{v}), \tag{B 7}$$

$$p_2 = 0 \quad \text{for } \boldsymbol{r} \in \partial V_1, \tag{B 8}$$

$$\alpha p_2 + \boldsymbol{n} \cdot \boldsymbol{D} \cdot \nabla p_2 = 0 \quad \text{for } \boldsymbol{r} \in \partial V_2. \tag{B 9}$$

A scalar product in $\mathscr{F}$ is defined as follows

$$(p_1, p_2) = -\int_V p_1 \nabla \cdot (\boldsymbol{D} \cdot \nabla p_2^*)\, \mathrm{d}V, \tag{B 10}$$

where the star denotes complex conjugate. All the necessary properties of a complex scalar product are satisfied. In particular, the divergence theorem and the boundary conditions for $p \in \mathscr{F}$ imply

$$(p,p) = \int_{\partial V_2} \alpha |p|^2 \,\mathrm{d}S + \int_V \nabla p \cdot \boldsymbol{D} \cdot \nabla p^* \,\mathrm{d}V > 0. \tag{B 11}$$

The operator A is antisymmetric with respect to the scalar product (B 10). Indeed, the definitions (B 7)–(B 10) yield

$$(Ap_1, p_2) + (p_1, Ap_2) = -\int_V p_2^* \nabla \cdot (p_1 \boldsymbol{v})\, \mathrm{d}V - \int_V p_1 \nabla \cdot (p_2^* \boldsymbol{v})\, \mathrm{d}V. \tag{B 12}$$

The condition (B 3) and the divergence theorem simplify the right-hand side of (B 12) to

$$-\int_{\partial V_1 \cup \partial V_2} p_1 p_2^* \boldsymbol{v} \cdot \boldsymbol{n}\, \mathrm{d}S, \tag{B 13}$$

which equals zero, according to (B 6) and the boundary conditions for $p_1, p_2 \in \mathscr{F}$. The spectral problem is equivalent to $p = Pe\,Ap$, and all the eigenvalues of an antisymmetric operator are always purely imaginary (Bellman 1970).

Unfortunately, this proof does not hold for our coalescence problem, owing to $\nabla \cdot \boldsymbol{v} \neq 0$, except for the case of an extremely small size ratio, when a small particle or drop tends to move along the streamlines past a large one. However, the scheme (B 1)–(B 6) includes a large number of other problems, e.g. the steady convective diffusion to an arbitrary-shaped particle (or a collection of particles) in an incompressible flow (Gupalo, Polyanin & Ryazantsev 1985), when the far-field boundary condition for the concentration is imposed on some remote, but finite computational boundary. Hence, the efficient method of §3.2 is applicable to these problems. If the spectrum slightly deviates from the imaginary axis due to finite-difference or Galerkin approximation, the number of nodes and/or the number of basis functions should be large enough to make the expansion in powers of w convergent for $Pe \leqslant Pe_m$.

Appendix C. Additional details

The familiar substitution (Acrivos & Taylor 1962)

$$p = 1 + \mathrm{e}^{-Pez/2} C, \quad z = s\cos\theta, \tag{C 1}$$

reduces (4.1) to

$$\nabla^2 C - \tfrac{1}{4} Pe^2\, C = 0. \tag{C 2}$$

The solution for the standard equation (C 2) can be found by separating variables,

$$C(s,\theta) = \sum_{n=0}^{\infty} C_n\, R_n\left(\frac{Pe\, s}{2}\right) P_n(\cos\theta), \tag{C 3}$$

where

$$R_n(x) = \left(\frac{\pi}{2x}\right)^{1/2} K_{n+1/2}(x) \tag{C 4}$$

is the modified spherical Bessel function ($K_{n+1/2}$ being the McDonald function of the order $n+\frac{1}{2}$). *Let* d_n be the Legendre coefficients for $\exp(Pe\,x)$, i.e.

$$\mathrm{e}^{Pex} = \sum_{n=0}^{\infty} d_n\, P_n(x) \quad \text{for } -1 \leqslant x \leqslant 1, \tag{C 5}$$

$$d_n = \tfrac{1}{2}(2n+1) \int_{-1}^{1} \mathrm{e}^{Pex} P_n(x)\, \mathrm{d}x. \tag{C 6}$$

The relations (C 1) and (C 3) yield the solution of the problem (4.1)–(4.3), if

$$C_n = -d_n / R_n(Pe). \tag{C 7}$$

According to (4.2) and (C 1), the collision efficiency for the Smoluchowski model is

$$E = \frac{2}{Pe} \int_0^{\pi} \mathrm{e}^{-Pe\cos\theta} \left.\frac{\partial C}{\partial s}\right|_{s=2} \sin\theta\, \mathrm{d}\theta. \tag{C 8}$$

Substituting (C 3) and (C 7) into (C 8) and using the properties of Legendre polynomials, we have

$$E = \sum_{n=0}^{\infty} (-1)^{n-1} \frac{2}{2n+1} d_n^2 \frac{R_n'(Pe)}{R_n(Pe)}. \tag{C 9}$$

The properties of R_n and P_n (Abramowitz & Stegun 1972) yield the relations

$$\frac{R_n'(Pe)}{R_n(Pe)} = -\left[\phi_n + \frac{n+1}{Pe}\right], \quad \phi_o = 1, \quad \phi_{n+1} = \frac{1}{\phi_n + (2n+1)/Pe}, \tag{C 10}$$

$$d_o = \frac{\sinh(Pe)}{Pe}, \quad d_1 = \frac{3}{Pe}\left[\cosh(Pe) - \frac{\sinh(Pe)}{Pe}\right], \tag{C 11}$$

$$d_n = Pe\left(\frac{d_{n-1}}{2n-1} - \frac{d_{n+1}}{2n+3}\right). \tag{C 12}$$

The form (C 9)–(C 12) of the solution was used in our calculations for table 1, with very fast convergence for small Pe. While formally exact for the model (4.1)–(4.3), this representation is, however, impractical when $Pe \geqslant O(10)$, because of a rapid loss of accuracy in summing up (C 9).

The simplification (4.1) of FP equation is also helpful for understanding the properties of the exact solution, with full hydrodynamic interactions. First, this simplification always holds at large distances, since the functions L, M, G and H can be replaced by unity and the van der Waals attraction neglected for $s \gg 1$. Hence, for $s \gg 1$, the solution has the form (C 3), even though the coefficients C_n have no connection to the inner boundary condition. Using the asymptotic result (Abramowitz & Stegun 1972),

$$R_n(x) \simeq \frac{\pi}{2x} e^{-x} \quad \text{for } x \to \infty, \tag{C 13}$$

we arrive at the far-field representation

$$p = 1 + \frac{1}{s}\exp(-Pe\, s(1+\cos\theta)/2)\, F(\cos\theta), \tag{C 14}$$

$$F(\mu) = \frac{\pi}{Pe}\sum_{n=0}^{\infty} C_n P_n(\mu), \tag{C 15}$$

valid for any finite Pe, when $s \to \infty$. As expected, the approach to unity when $s \to \infty$ is exponential everywhere, except in the wake $\cos\theta \approx -1$. The Legendre coefficients (3.1) can be obtained from (C 14):

$$a_n = \delta_{n,0} + \frac{(2n+1)}{2s}\int_{-1}^{1} \exp(-Pe\, s(1+\mu)/2)\, F(\mu)\, P_n(\mu)\, \mathrm{d}\mu. \tag{C 16}$$

According to the Laplace method, the function $F(\mu)\, P_n(\mu)$ for $s \gg 1$ can be replaced by $F(-1)\, P_n(-1) \neq 0$ and the upper integration limit by ∞, implying the $O(s^{-1})$ estimate for the integral (C 16). Thus, for fixed n and $Pe \neq 0$, the coefficient a_n behaves like $\delta_{n,0} + O(s^{-2})$ when $s \to \infty$, as was stated in §3.1. Interestingly, the asymptotic structure of the solution described in §4 yields the same behaviour of a_n for $Pe = \infty$.

Finally, the simplification (4.1) allows us to study how the radius h of convergence of (3.21) behaves, when the position $s = s_I$ of the outer boundary tends to infinity. Indeed, when estimating h for $s_I \gg 1$, it seems plausible to neglect a relatively small region, $s - 2 \leqslant O(1)$, where the approximation (4.1) is invalid. So, the eigenvalue problem for $p = \exp(-Pe\, z/2)\, C$ simplifies to

$$\nabla^2 C - \frac{Pe^2}{4} C = 0, \quad C|_{s=s_I} = 0. \tag{C 17}$$

The inner boundary condition is lost and replaced by a regularity of C at $s = 0$. Substitution $Pe = ih$ yields the eigenfunction

$$C = \frac{1}{s}\sin(\tfrac{1}{2}hs) \tag{C 18}$$

with the minimum possible $h = 2\pi/s_I$. Albeit not quite rigorously derived, the asymptotic result $h \simeq 2\pi/s_I$ for $s_I \to \infty$ is completely confirmed by our numerical calculations.

Appendix D. On the retarded van der Waals interaction between two spheres

In order to integrate the interaction energy (6.7) and (6.8) over the volumes V_1 and V_2 of the two spheres of radii a_1 and a_2 with centre-to-centre distance r, consider the integrals

$$I_n(a_1, a_2, r) = \int_{V_1}\int_{V_2} \frac{dV_1\, dV_2}{\rho^n} \tag{D 1}$$

for integers $n \geqslant 6$. Expanding I_n as a double series in powers of a_1 and a_2, one can derive

$$\frac{\partial}{\partial r}(rI_n) = -(n-1)rI_{n+1}. \tag{D 2}$$

Hence, the explicit expressions for I_n with $n \geqslant 7$ can be obtained, starting from the Hamaker integral I_6 (see (6.4)):

$$I_n = \frac{4\pi^2}{(n-2)!\,r^{n-6}} J_n, \tag{D 3}$$

$$\begin{aligned} J_n = {} & (n-6)!\left[\frac{1}{(1-\alpha_1-\alpha_2)^{n-5}} + \frac{1}{(1+\alpha_1+\alpha_2)^{n-5}} + \frac{1}{(1+\alpha_1-\alpha_2)^{n-5}} + \frac{1}{(1-\alpha_1+\alpha_2)^{n-5}}\right]\alpha_1\alpha_2 \\ & + (n-7)!\left[\frac{\alpha_1-\alpha_2}{(1+\alpha_2-\alpha_1)^{n-6}} + \frac{\alpha_2-\alpha_1}{(1+\alpha_1-\alpha_2)^{n-6}} + \frac{\alpha_1+\alpha_2}{(1+\alpha_1+\alpha_2)^{n-6}} - \frac{(\alpha_1+\alpha_2)}{(1-\alpha_1-\alpha_2)^{n-6}}\right] \\ & + f_n(\alpha_1+\alpha_2) + f_n(-\alpha_1-\alpha_2) - f_n(\alpha_2-\alpha_1) - f_n(\alpha_1-\alpha_2), \end{aligned} \tag{D 4}$$

where $\alpha_i = a_i/r$ and

$$f_n(x) = (n-8)!/(1+x)^{n-7} \quad \text{for } n \geqslant 8, \tag{D 5}$$

$$f_n(x) = -\ln(1+x) \quad \text{for } n = 7. \tag{D 6}$$

By using (6.7) and (6.8) and (D 1)–(D 6), the dimensionless interparticle potential $\phi = \Phi_{12}/A$ and its derivative $\phi'(s)$ take the form

$$\phi = -\frac{1}{60}\left[2.45\Omega J_7 - \frac{2.17}{12}\Omega^2 J_8 + \frac{0.59}{168}\Omega^3 J_9\right], \tag{D 7}$$

$$\phi'(s) = \frac{(\alpha_1+\alpha_2)}{120}\left[2.45\Omega(J_7+J_8) - \frac{2.17}{12}\Omega^2(J_8+J_9) + \frac{0.59}{168}\Omega^3(J_9+J_{10})\right], \tag{D 8}$$

where $\Omega = \lambda_L/(\pi r)$.

REFERENCES

ABRAMOWITZ, M. & STEGUN, I. A. 1972 *Handbook of Mathematical Functions*. Dover.

ACRIVOS, A. & TAYLOR, T. D. 1962 Heat and mass transfer from single spheres in Stokes flow. *Phys. Fluids* **5**, 387–394.

BATCHELOR, G. K. 1976 Brownian diffusion of particles with hydrodynamic interaction. *J. Fluid Mech.* **74**, 1–29.

BELLMAN, R. E. 1970 *Introduction to Matrix Analysis*. McGraw–Hill.

CLAYFIELD, E. J., LUMB, E. C. & MACKEY, P. H. 1971 Retarded dispersion forces in colloidal particles – exact integration of the Casimir and Polder equation. *J. Colloid Interface Sci.* **37**, 382–389.

COLE, J. 1968 *Perturbation Methods in Applied Mathematics*. Ginn–Blaisdell.

DAVIS, R. H. 1984 The rate of coagulation of a dilute polydisperse system of sedimenting spheres. *J. Fluid Mech.* **145**, 179–199.

DAVIS, R. H., SCHONBERG, J. A. & RALLISON, J. M. 1989 The lubrication force between two viscous drops. *Phys. Fluids* A **1**, 77–81.

FEKE, D. L. & SCHOWALTER, W. R. 1983 The effect of Brownian diffusion on shear-induced coagulation of colloidal dispersions. *J. Fluid Mech.* **133**, 17–35.

GUPALO, YU. P., POLYANIN, A. D. & RYAZANTSEV, YU. S. 1985 *Mass and Heat Transfer from Reacting Particles to a Flow*. Moscow: Nauka (in Russian).

HABER, S., HETSRONI, G. & SOLAN, A. 1973 On the low Reynolds number motion of two droplets. *Intl J. Multiphase Flow* **1**, 57–71.

HAMAKER, H. C. 1937 The London–van der Waals attraction between spherical particles. *Physica* **4**, 1058.

HO, N. F. H. & HIGUCHI, W. I. 1968 Preferential aggregation and coalescence in heterodispersed system. *J. Pharm. Sci.* **57**, 436–442.

KIM, S. & FAN, X. 1984 A perturbation solution for rigid dumbbell suspensions in steady shear flow. *J. Rheol.* **28**, 117–122.

KIM, S. & ZUKOVSKI, C. F. 1990 A model of growth by hetero-coagulation in seeded colloidal dispersions. *J. Colloid Interface Sci.* **139**, 198–212.

LAMB, S. H. 1945 *Hydrodynamics*, p. 600. Dover.

LANGBEIN, D. 1974 *Theory of van der Waals Attraction*. Springer.

MELIK, D. H. & FOGLER, H. S. 1984*a* Effect of gravity on Brownian flocculation. *J. Colloid Interface Sci.* **101**, 84–97.

MELIK, D. H. & FOGLER, H. S. 1984*b* Gravity-induced flocculation. *J. Colloid Interface Sci.* **101**, 72–83.

PRIEVE, D. C. & RUCKENSTEIN, E. 1974 Effect of London forces upon the rate of deposition of Brownian particles. *AIChE J.* **20**, 1178–1187.

REED, L. D. & MORRISON, F. A. 1974 The slow motion of two touching fluid spheres along their line of centers. *Intl J. Multiphase Flow* **1**, 573–583.

RUSHTON, E. & DAVIES, G. A. 1973 The slow unsteady settling of two fluid spheres along their line of centers. *Appl. Sci. Res.* **28**, 37–61.

SCHENKEL, J. H. & KITCHENER, J. A. 1960 A test of the Derjaguin–Verwey–Overbeek theory with a colloidal suspension. *Trans. Faraday Soc.* **56**, 161–173.

SPIELMAN, L. A. 1970 Viscous interactions in Brownian coagulation. *J. Colloid Interface Sci.* 562–571.

VALIOULIS, I. A. & LIST, E. J. 1984 Collision efficiencies of diffusing spherical particles: hydrodynamic, van der Waals and electrostatic forces. *Adv. Colloid Interface Sci.* **20**, 1–20.

VAN DYKE, M. 1974 Analysis and improvement of perturbation series. *Q. J. Mech. Appl. Maths* **27**, 423–450.

WANG, Y. G. & WEN, C. S. 1990 The effect of weak gravitational force on Brownian coagulation of small particles. *J. Fluid Mech.* **214**, 599–610.

WANG, H., ZINCHENKO, A. Z. & DAVIS, R. H. 1994 The collision rate of small drops in linear flow field. *J. Fluid Mech.* **265**, 161–188.

WEN, C.-S. & BATCHELOR, G. K. 1985 The rate of coagulation in a dilute suspension of small particles. *Scientia Sinica* A **28**, 172–184.

ZHANG, X. & DAVIS, R. H. 1991 The rate of collisions due to Brownian or gravitational motion of small drops. *J. Fluid Mech.* **230**, 479–504.

ZINCHENKO, A. Z. 1978 Calculation of hydrodynamic interactions between drops at low Reynolds number. *Prikl. Mat. Mech.* **42**, 1046–1051.

ZINCHENKO, A. Z. 1980 The slow asymmetric motion of two drops in a viscous medium. *Prikl. Mat. Mech.* **44**, 30–37.

ZINCHENKO, A. Z. 1982 Calculations of the effectiveness of gravitational coagulation of drops with allowance for internal circulation. *Prikl. Mat. Mech.* **46**, 58–65.